



**ALL-OPTICAL LOGIC GATES AND WAVELENGTH CONVERSION VIA THE
INJECTION-LOCKING OF A FABRY-PEROT SEMICONDUCTOR LASER**

THESIS

Evan P. Harvey, Second Lieutenant, USAF

AFIT-ENG-13-M-23

**DEPARTMENT OF THE AIR FORCE
AIR UNIVERSITY**

AIR FORCE INSTITUTE OF TECHNOLOGY

Wright-Patterson Air Force Base, Ohio

**DISTRIBUTION STATEMENT A.
APPROVED FOR PUBLIC RELEASE; DISTRIBUTION UNLIMITED**

The views expressed in this thesis are those of the author and do not reflect the official policy or position of the United States Air Force, Department of Defense, or the United States Government.

**ALL-OPTICAL LOGIC GATES AND WAVELENGTH CONVERSION VIA THE
INJECTION-LOCKING OF A FABRY-PEROT SEMICONDUCTOR LASER**

THESIS

Presented to the Faculty

Department of Electrical and Computer Engineering

Graduate School of Engineering and Management

Air Force Institute of Technology

Air University

Air Education and Training Command

In Partial Fulfillment of the Requirements for the
Degree of Master of Science in Electrical Engineering

Evan P. Harvey, B.S.E.E.

Second Lieutenant, USAF

March 2013

**DISTRIBUTION STATEMENT A.
APPROVED FOR PUBLIC RELEASE; DISTRIBUTION UNLIMITED**

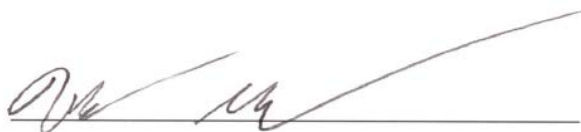
**ALL-OPTICAL LOGIC GATES AND WAVELENGTH CONVERSION VIA THE
INJECTION-LOCKING OF A FABRY-PEROT SEMICONDUCTOR LASER**

Evan P. Harvey, B.S.E.E.
Second Lieutenant, USAF

Approved:

 3/5/2013

Michael C. Pochet, Maj, Ph.D. (Chairman) Date

 03/04/2013

Nicholas G. Usechak, Ph.D. (Member) Date

 03/04/2013

Derrick Langley, Capt, Ph.D. (Member) Date

Abstract

This work investigates the implementation of all-optical wavelength conversion and logic gates based on optical injection locking (OIL). All-optical inverting, NOR, and NAND gates are experimentally demonstrated using two distributed feedback (DFB) lasers, a multi-mode Fabry–Perot laser diode (MMFP-LD), and an optical band-pass filter (BPF). The DFB lasers are externally modulated to represent logic inputs into the cavity of the MMFP-LD slave laser. The master lasers' wavelengths are aligned with the longitudinal modes of the MMFP-LD slave laser and their optical power is used to modulate the injection conditions in the slave laser. The optical BPF is used to select the longitudinal mode that is suppressed or transmitted given the logic state of the injecting master laser signals. When the input signal(s) is (are) in the on state, injection locking, and thus the suppression of the non-injected Fabry–Perot modes, is induced, yielding a dynamic system that can be used to implement photonic logic functions. Additionally, all-optical photonic processing is achieved using the cavity mode shift produced in the injected slave laser under external optical injection. The inverting logic case can also be used as a wavelength converter — a key component in advanced wavelength-division multiplexing networks. The result of this experimental investigation is a more comprehensive understanding of the locking parameters concerning the injection of multiple lasers into a multi-mode cavity. Attention is placed on the turn-on/turn-off transition dynamics, along with the maximum achievable bit rates. The performance of optical logic computations and wavelength conversion has the potential for ultrafast operation, limited primarily by the photon decay rate in the slave laser.

To my wife and family. Thank you for all of your support.

Acknowledgments

I would first like to express my gratitude to my research advisor, Maj. Michael C. Pochet, for sharing his extensive knowledge of optical communications. Without his direction, much of my work would not have been possible. Additionally, I would like to express my thanks to my committee member, Dr. Nicholas G. Usechak, for providing me with the laboratory space to test all of the experiments described here and for taking time to answer questions concerning my work. His contributions to this document were invaluable and I sincerely thank him for entrusting me with about a quarter million dollars worth of his lab equipment. I would like to thank Capt. Derrick Langley for reading my documentation and taking the time to be a part of my committee. I would like to also acknowledge John Schmidt; since I had relatively no experience using laboratory equipment, his help in the laboratory was crucial to my success. Most importantly, I would like to thank my wife for always being supportive of me at home. Without her encouragement, none of this research would have been possible.

Evan P. Harvey

Table of Contents

	Page
Abstract	iv
Acknowledgments.....	1
Table of Contents	2
List of Figures	4
List of Tables	7
1. Introduction	8
1.1 Communications Challenges	8
1.2 Importance of Photonic Signal Processing	10
1.3 Experimental Overview	16
1.4 Research Goals and Justification	16
1.5 Research Goals and Justification	17
2. Literature Review	18
2.1 Optical Communications	18
2.2 Optical Injection	22
2.2.1 Injection Stabilities and Dynamics	24
2.2.2 Rate Equations	26
2.2.3 Optical Injection Enhancements	32
2.3 Wavelength Conversion and Optical Logic	34
2.3.1 Mode Suppression Based Logic	36
2.3.2 Wavelength Conversion via Mode Shift.....	39
2.3.3 Single-Mode Fabry–Perot Logic	50
2.4 Literature Review Conclusion	55
3. Methodology	56
3.1 Laboratory Setup	57
3.1.1 Wavelength Conversion and NOT Gate	57
3.1.2 NOR and NAND Gate	60
3.2 Experiments	63
3.2.1 Mode Suppression Method	63
3.2.2 Cavity Mode Shift Method	63
3.2.3 Cavity Mode Shift Speed Limitations	64
3.2.4 NOR/NAND Gate Measurements	64

3.3	Equipment.....	65
3.3.1	Laboratory Lasers	66
3.3.2	Measuring and Analysis Equipment.....	67
3.3.3	Mach-Zehnder Modulator.....	68
3.3.4	Optical Circulator	70
3.4	Methodology Summary	71
4.	Analysis and Results	72
4.1	Mode Suppression Results.....	74
4.2	Cavity Mode Shifting Results.....	79
4.3	NOR Gate Results.....	85
4.4	NAND Gate Results	88
4.5	Summary of Findings	91
5.	Conclusions and Recommendations.....	92
5.1	Conclusions of Research.....	92
5.2	Contributions	94
5.3	Recommendations for Future Research.....	95
	References.....	99

List of Figures

	Page
Figure 1: Optical-electrical-optical method of wavelength conversion.....	11
Figure 2: One of the proposed optical-optical methods of wavelength conversion. ...	12
Figure 3: Physical illustration of optical injection.....	14
Figure 4: Optical Spectrum of a Fabry–Perot laser injection-locked (red) and free-running (blue).	15
Figure 5: Cavity modes of a Fabry–Perot resonator superimposed over the gain spectrum/Lorentzian model estimate [8].....	23
Figure 6: Experimentally obtained map of observed optical injection states in relation to the detuning frequency, f , and normalized injection parameter, ξ . States labeled are: (S) stable, (P1) period one, (P2) period doubling, (P4) period quadrupling, (4) four wave mixing, (M) multi-wave mixing, and chaos (shaded regions) [10].....	25
Figure 7: Optical logic inverter. The devices used are labeled as follows; MLD (master laser diode), SLD (slave laser diode), EOM (electro-optic modulator), P (polarizer), OI (optical isolator), G (grating), L (lens), BE (beam expander), and PD1 PD2 (photodiodes) [24].	37
Figure 8: Fall (a) and rise (b) time of the inverted output of the logic gate described in Figure 7 [24].....	38
Figure 9: Example locking range of an optically injected laser. (a) Unlocked (b) stably locked (c) locked with the slave mode still present and (d) unlocked [32].	41
Figure 10: Illustration depicting wavelength conversion using cavity shifting properties with the bars depicting laser modes in the optical spectrum. (a) The free-running slave laser with arbitrary modes, ν_m and ν_n . (b) Injection of probe beam, ν_p . (c) Additional injection of data beam, ν_d , and detuning frequencies, $\Delta\nu_1$ and $\Delta\nu_2$ [25].	42
Figure 11: Numerically calculated extinction ratio for wavelength converter based on cavity mode shifting. Dashed line represents the results for a cavity length of 420 μm . Solid line represents cavity mode of 250 μm . The inset eye diagram is calculated for a 250 μm at a data rate of 10 Gbps [25].	44

Figure 12: Optical spectrum of an all-optical NOR gate. Grey dotted line represents injection under the probe beam only. (a) No data is injected. (b) and (c) only one data beam is injected. (d) Both data signals are injected [23].	46
Figure 13: (a) The optical intensity output when injected beam is TE polarized for several detuning frequencies. (b) Output when injected beam is TM polarized [35].	47
Figure 14: Shift of Fabry–Perot modes by injection of a TE mode and the effects on the TM polarized probe beam[38].	48
Figure 15: The operation of the all-optical bit error rate monitor. (i) The original signal with errors. (ii) The output of the NOT gate operating with the Γ_{low} threshold. (iii) NOR output of inverted and original signals using the Γ_{high} threshold[40].	49
Figure 16: An example of a Fabry–Perot laser diode with an external cavity [41].	50
Figure 17: Optical spectrum of XNOR gate. A and B are data signals, C is the NAND output of A and B, and E is the XNOR output of A and B. (a) A = 0, B = 0, C = 1, E = 1. (b) A = 0, B = 1, C = 1, E = 0. (c) A = 1, B = 0, C = 1, E = 0 (d) A = 1, B = 1, C = 0, E = 1 [46].	53
Figure 18: An all-optical half-adder involving all-optical NAND, AND, XNOR, and XOR gates [44].	54
Figure 19: Experimental setup of a wavelength converter/NOT gate dependent on side-mode suppression.	58
Figure 20: Experimental setup of an all-optical NOT gate/wavelength converter utilizing cavity mode shifting with an external CW probe beam.	59
Figure 21: Experimental setup of an all-optical NOR/NAND gate utilizing an external CW probe beam.	61
Figure 22: Illustration of signal generation for all-optical logic gates.	62
Figure 23: An example of a closed eye diagram (left) and an open eye diagram (right) [8].	68
Figure 24: Experimentally obtained measurements of Mach-Zehnder external modulator optical power output versus the DC bias voltage.	69
Figure 25: Optical injection with a single-mode DFB into a slave Fabry–Perot cavity causing a suppression of adjacent side modes.	74

Figure 26: Oscilloscope results for modulation at 100 Mbps, 500 Mbps, and 1 Gbps. The top row (a) of results show a 16 bit input waveform of 0000101010101010. The bottom row (b) uses a pattern of 1111101010101010.....	75
Figure 27: Left eye diagram (a) 100 Mbps PRBS input signal and (b) inverted output signal using mode suppression. Right eye diagram (c) 1 Gbps PRBS input signal and (d) inverted output signal using mode suppression.	77
Figure 28: Optical spectrum of an all-optical inverter using a CW probe beam. (a) Optical spectrum of an unlocked MMFP-LD (b) Slave laser under injection from the CW probe only (c) Injection of data signal and probe. .	80
Figure 29: Waveforms generated using the cavity mode shift method. The top row (a) of results show a 16 bit input waveform of 1111010101010101. The bottom row (b) uses a pattern of 0000101010101010.	81
Figure 30: Eye diagram of probe beam (a) 12.5 Gbps PRBS input signal and (b) inverting output signal.	82
Figure 31: Left eye diagram (a) 1 Gbps PRBS input signal and (b) inverted output signal using mode suppression. Right eye diagram (c) 1 Gbps PRBS input signal and (d) inverted output signal using cavity mode shifting.	83
Figure 32: Probe beam wavelength conversion/inversion using a 19 GHz sinusoid...	84
Figure 33: Optical spectrum of NOR gate. Injected lasers indicated in legend induce the following logical outputs: (a) '1', (b) '0', (c) '0', and (d) '0'..	86
Figure 34: Input signals and output of all-optical NOR gate.....	87
Figure 35: Optical spectrum of NAND gate. Injected lasers indicated in legend induce the following logical outputs: (a) '1', (b) '1', (c) '1', and (d) '0'..	89
Figure 36: Input signals and output for all-optical NAND gate at 3 Gbps.	90

List of Tables

	Page
TABLE 1: A list of limitations to directly modulated semiconductor lasers and their respective improvements due to optical injection [9].	33
TABLE 2: List of standard binary logic truth tables.	45

ALL-OPTICAL LOGIC GATES AND WAVELENGTH CONVERSION VIA THE INJECTION-LOCKING OF A FABRY–PEROT SEMICONDUCTOR LASER

1. Introduction

This document aims to investigate all-optical logic capabilities based on optically injected Fabry–Perot semiconductor lasers. Advancing communications capabilities using the principles of fiber optic communications and optical-injection locking is the primary motivation driving this research. Optical signal processing is a developing field that hopes to advance communications technology by taking advantage of the physical characteristics of light. The research will work to analyze the dynamics of optically-injected wavelength conversion and logic, and experimentally investigate the modulation limits of these injection-locking-based approaches. If this research is successful, it will contribute to the understanding of photonic signal processing. The purpose of this chapter is to justify the importance of this research by outlining the problems concerning modern fiber-optic communications infrastructure. Additionally, this document is intended to describe research goals and provide a background to the topics involved. It is the intent of this manuscript that these results will provide a path toward developing photonic components that can be integrated with current semiconductor-based circuits.

1.1 Communications Challenges

The need for a higher capacity communications infrastructure poses a critical engineering challenge for 21st century. Due to exponentially increasing communications needs, fiber-optics use has now surpassed that of copper wire

networks. The capacity of single-mode optical fibers has increased 10,000 fold since it was initially introduced nearly three decades ago. Thankfully, over this same time period, network traffic has witnessed only a 100 fold increase [1]. These statistics would lead one to believe that optical fiber can meet modern communication challenges. Unfortunately, increases in fiber capacity have drastically slowed, while demand has dramatically increased. With the constant addition of cellular phones, tablets, and a number of other electronic devices that can connect to the internet, it is obvious that this trend will not be losing momentum in the foreseeable future. Essentially, technology increases have slowed while communications demands have been increasing exponentially [1].

Modern communication innovations are based on the advantages of using light as a transmission medium. Traditionally, wires use the flow of electrons to send communication signals. With the advent of fiber optics, an electrical signal generated by an end user can be transformed to an optical signal that can be propagated along a fiber-optic cable to the receiver. While optical signals travel significantly faster than electrical signals through a coaxial cable (roughly 80% the speed of light), the key attractiveness of optical-fiber communications lies in its extremely low attenuation level, along with its dramatically higher bandwidths when compared to copper cables. Additionally, optical-fiber transmission lines are much cheaper than copper wires when used for long distances. Laser diodes are used to create the signal at the transmitter. Optical signals transfer information using *on-off keying* (OOK), *amplitude shift-keying* (ASK), or other formats as the modulation scheme. For example, with an OOK modulation scheme, when the laser is on, the signal is high indicating a binary

‘1’; when the beam is blocked or off, the signal is low, or ‘0’. While this optical signal is cost effective and efficient, it must still be converted to and from an electrical format if the signal is communicating with any transistor-based device, such as a computer. If electrical devices could be better integrated with or possibly replaced by these photonic signals, communication capacity, and information processing speeds would be increased significantly. Developing a low-power method of performing logic functions utilizing optical signals would work toward the objective of better integrating optical signals. The goal of performing logic using photons contributes to the fields of optical signal processing, optical networking, optical logic, and optical computing.

1.2 Importance of Photonic Signal Processing

For the most part, optical signals are primarily used in long-distance communications. Recently, fiber-optic cables have become more prevalent in shorter distance applications; many commercially available household surround-sound systems use fiber-optic connectors. Even shorter distance applications, such as chip-to-chip optical connections, are being explored. A 70 percent increase in speed and efficiency is feasible when utilizing optical chip-to-chip interconnects [2]. There are obvious incentives towards replacing more electrical-based connections with optical connections. The most radical innovation would be a partial, or even complete, replacement of electrical components at the board level or further to the chip level.

When considering improvements to long-haul communication networks, one method of improving data capacity is through wavelength-division multiplexing

(WDM). Using this technique, multiple signals of varying wavelengths are combined onto a single fiber. The various optical channels are regulated and defined by the International Telecommunications Union (ITU); these standardized bands are referred to as ITU bands and are analogous to the frequency bands defined by the Federal Communications Commission (FCC). In the course of transmission, it may be required that a signal be converted from one ITU channel to another. The standard wavelength conversion process is illustrated in Figure 1.

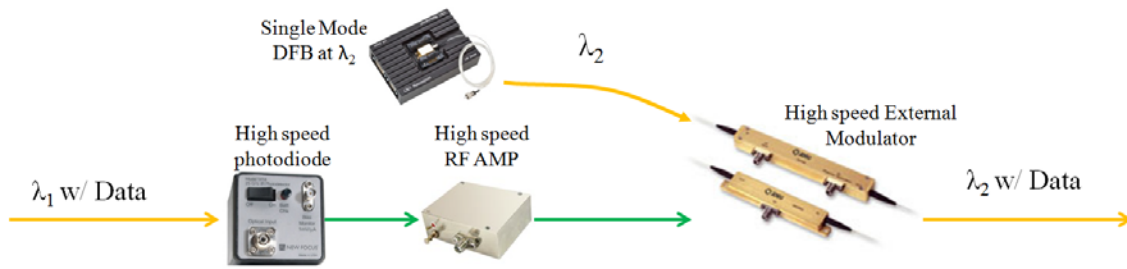


Figure 1: Optical-electrical-optical method of wavelength conversion.

As illustrated in Figure 1, the standard wavelength conversion process is an optical-to-electrical-to-optical process. In transferring a baseband signal from one carrier wavelength, the input optical signal is passed through a photodetector where the baseband signal is detected and converted to an electrical signal. The electrical signal is amplified using a high-speed microwave amplifier such that it can provide an adequate voltage swing to operate an external modulator. External modulators commonly require large peak-to-peak voltage swings to attain a suitable modulation depth of the output optical signal. Additionally, a second single-mode transmitting laser is needed to generate the carrier signal that is sent to the external modulator. The

optical-to-electrical-to-optical concept presents an expensive solution to wavelength conversion given that high bandwidths (> 26 GHz to account for the first three Fourier series harmonics of a 10-Gbps square wave) are required for the integrated electrical components.

The approach described in this document presents an all-optical method to achieve wavelength conversion and optical logic, outlined here in Figure 2. In this method, the data is passed through an optical circulator to a Multi-Mode Fabry–Perot laser diode (MMFP-LD), after which the output wavelength is selected using an optical band-pass filter (BPF). This process is essentially an optical-to-optical conversion. Comparing the conventional optical-to-electrical-to-optical approach for wavelength conversion illustrated in Figure 1 to the all-optical approach laid out in Figure 2, it can be observed that the need for high bandwidth RF components is eliminated; the approach in Figure 2 is based on passive optical elements (optical circulator & optical bandpass filter) and a Fabry–Perot semiconductor laser that requires only a DC current bias. The devices and physics contributing to these approaches are the primary subject of this document.



Figure 2: One of the proposed optical-optical methods of wavelength conversion.

Modern computers use transistors as their basic logical component. These transistors can be arranged to create logic gates, components that perform logical processes with electrons. Integrated circuits can contain billions of transistors, and have been responsible for exponentially increasing the ability to process and share information. A revolutionary accomplishment would be the development of a computer that can perform logical functions using only photons, but current technology is far from a level of technological maturity that could compete with integrated circuits. Performing logic functions using light is an important first step toward this goal. This process involves the creation of an all-optical logic gate.

Several theories, techniques, and devices have been developed that perform logic functions using photons. Some of these developments include photonic crystals, semiconductor optical amplifiers [3], and Erbium-doped optical fiber amplifiers [4]. One possible technique used to perform photonic logic as well as wavelength conversion is *optical injection locking* (OIL). OIL is a process that involves two coupled lasers, referred to as the slave and master laser based on their coupling arrangement. Figure 3 shows a physical interpretation of optical injection, whereby the master laser is injected into the resonance cavity of the slave laser; an optical isolator is placed between the master and slave lasers to prevent to dual coupled system. If injected at a suitable power level and wavelength, the slave laser mode(s) lock to the wavelength of the master laser.

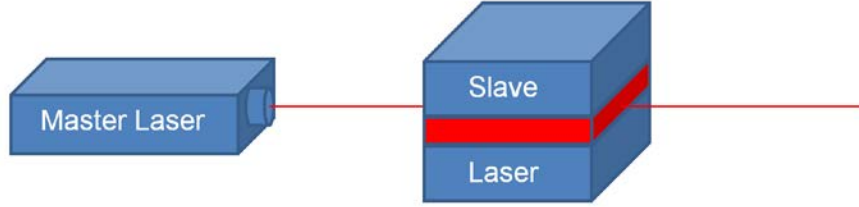


Figure 3: Physical illustration of optical injection.

OIL has been thoroughly investigated over the past three decades due to its ability to improve a semiconductor laser's free-running parameters including: single-mode operation with a large side-mode suppression ratio (SMSR), improved modulation bandwidths, reduced linewidth, better relative intensity noise, and lower chirp [5]. The OIL-induced improvements to laser operation are typically investigated for implementations in coherent optical communication system transmitters for the purpose of increasing modulation bandwidths and suppressing the deleterious effects of chromatic dispersion in order to enhance the bit-rate-distance product of directly modulated semiconductor lasers [6, 7, 8]. Additionally, OIL induces a shift in the cavity mode; this shift is a result of changes to the carrier concentration in the slave laser which occur because of the injected field [5, 9]. This manuscript takes advantage of the OIL characteristics of Fabry–Perot lasers to demonstrate wavelength conversion and optical logic gates.

A basic example of the optical power spectrum of a Fabry–Perot laser under stable OIL is given in Figure 4. In Figure 4, the key observable feature is the greater than 30-dB side-mode suppression ratio observed when the laser is injection locked. Although less noticeable in Figure 4, a red shift to the supported Fabry–Perot modes is

present in the injection locked spectrum when compared to the free-running modes of the Fabry–Perot laser.

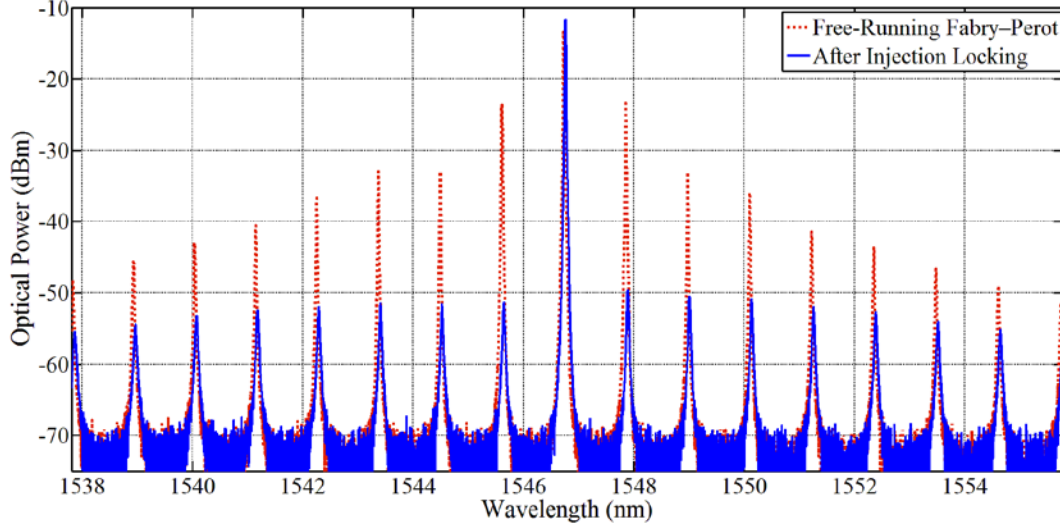


Figure 4: Optical Spectrum of a Fabry–Perot laser injection-locked (blue-solid) and free-running (red-dotted).

Optical injection locking and its implementation in both wavelength conversion schemes and logic gates will be discussed thoroughly in the literature review chapter. Compared with other logic operation implementation techniques, this technique involves inexpensive Fabry–Perot laser diodes, passive optical components, and is relatively easy to implement. The intent of this research is to evaluate implementation schemes capable of performing logic functions using optical injection locking. Focus is placed on investigating the maximum achievable bit rates for the implementation schemes under study.

1.3 Experimental Overview

In this work, specialized optical circuits have been constructed in order to observe and measure the operation of the wavelength converters and all-optical logic gates. Basic all-optical logic operations are described by the following: when injecting a single-mode laser into a multi-mode Fabry–Perot laser cavity, the side modes of the multi-mode laser will be suppressed and the only wavelength that will propagate will be that of the master laser; by band-pass filtering a non-injected mode, a ‘0’ will be seen when the master laser is transmitting a ‘1’; this interaction results in an inverted data signal, a function performed by a NOT gate; in addition to inverting the data signal, the wavelength is output at a new wavelength other than that of the injected signal. Other methods presented in this document make use of the cavity mode shift that occurs during injection locking. Prior literature suggests that injecting two single-mode, tunable, master lasers into a Fabry–Perot laser can suppress modes in different combinations [10]. Using this technique, literature suggests that AND, OR, NAND, NOR, XOR, and XNOR logic gates can all be created using only optical signals [11, 12].

1.4 Research Goals and Justification

Prior literature discussing wavelength conversion or optical logic strictly inspects the cavity mode shift method or makes use of a single-mode Fabry–Perot laser (SMFP-LD) [13]. While the limits of cavity mode shifting are thoroughly explored, the mode suppression method is a promising alternative with scarce experimental findings available in literature. Additionally, most optical injection

experiments have a single master laser; as a result there is a limited amount of experimental research involving multi-mode injection. These unique factors suggest that the data retrieved from this experiment are distinctive and will help to better define the behavior of injection-based logic gates. As a result of these investigations, it is the objective of this document to provide a more rigorous understanding of the principles governing the effects of multiple-beam optical injection on a multi-mode Fabry–Perot laser diode. This improved understanding can then be experimentally applied to gain insight into the performance of both all-optical wavelength conversion and all-optical logic gates.

1.5 Research Goals and Justification

The following document has been organized into five chapters. This first chapter is meant to introduce the topic and give a general overview of the techniques and disciplines incorporated in this thesis. Chapter two provides a literature review with the intention of summarizing the fields of optical communications, OIL, and photonic logic. The purpose of this chapter is to provide the reader with a summary of the current state of optical logic and the physics that are utilized in these experiments. Chapter three, the methodology section, provides a comprehensive description of the experiments that are performed and the equipment that is used. Chapter four will present the results of the experiments outlined in the methodology section while providing analysis on how these methods could possibly be improved. The last chapter will summarize the findings of this document and provide recommendations for further progress.

2. Literature Review

The purpose of this chapter is to provide a review of literature relating to subject matters explored in this thesis research. Topics presented in this section are relevant to the optical wavelength conversion of a signal and the creation of an all-optical logic gate using optical injection of Fabry–Perot lasers. First, a discussion of optical communications is necessary to understand how photon-based communication works. Next, optical injection is discussed thoroughly. The effects of optical injection are the principal focus of this research; therefore, it is important that the topic is covered in depth. This discussion includes an analysis of the different regions of stability that can be achieved and an overview of the rate equations governing the operation of semiconductor lasers under optical injection. Lastly, this chapter will review some of the literature that examines optical logic.

2.1 Optical Communications

In recent decades, optical fiber communications has replaced electrical systems as the primary means of communication for high data rates (> 100 Mbps) and substantial transmission distances (> 100 m) in modern environments. Single mode optical fibers, the common transmission medium for medium- to long-haul optical communications, possess bandwidths greater than 6.5 THz over the optical wavelength range from 1525 nm to 1575 nm. Moreover, the attenuation over this wavelength range is less than 0.2 dB per km [14]. Both the low attenuation per km and THz-range bandwidth make optical communication ideal when compared to standard copper-based coaxial communication architectures or wireless microwave communication

links. In one reported example, WDM and quadrature amplitude modulation (QAM) was used to achieve a record data rate of 101.7 Tb/s for a fiber-optic communication link over three 55-km spans of single-mode fiber [1, 15]. Additionally, fiber optics are not affected by electromagnetic interference since the data carrier is light. A signal traveling through an optical fiber cannot be detected outside of the fiber; therefore, the signal cannot be tapped without physically breaking the optical cable.

Though lasers are sometimes described as having a single wavelength, the gain spectrum of the pulse generated is actually Gaussian in shape and carries a continuum of wavelengths. As this pulse travels through a fiber, different frequencies of light will arrive at different times depending on the group velocity. This temporal spreading of the optical pulse is due to dispersion. The dispersion parameter, D , can be expressed as the sum of two specific types of dispersion, waveguide dispersion and material dispersion [14]. Material dispersion, D_M , occurs due to the frequency dependence of the index of the material. Waveguide dispersion, D_W , takes into account several waveguide parameters. The material and waveguide dispersions are described in equations (1) and (2) [14].

$$D_M = \frac{2\pi}{\lambda^2} \frac{dn_{2g}}{d\lambda} \quad (1)$$

$$D_W = -\frac{2\pi\Delta}{\lambda^2} \left[\frac{n_{2g}^2}{n_2} \frac{V d^2(Vb)}{dV^2} + \frac{dn_{2g}}{d\omega} \frac{d(Vb)}{dV} \right] \quad (2)$$

When the dispersion terms are summed they equal total dispersion, D , expressed in units of ps/(km-nm). Expressing the dispersion in these units allows the D parameter to be multiplied by the wavelength range and the distance traveled

resulting in a temporal spreading of the pulse, expressed in picoseconds. The amount of pulse broadening that occurs places a limit on the bit-rate-distance product, BL . The temporal spread and the effect of dispersion are shown in equations (3) and (4), respectively.

$$\Delta T = DL\Delta\lambda \quad (3)$$

$$BL|D|\Delta\lambda < 1 \quad (4)$$

It is evident by these equations that a narrowing of the spectrum of the pulse would lead to a reduction in the temporal spread of that pulse after propagation. If the dispersion can be reduced, then a better bit-rate-distance product can be achieved.

Optical systems make use of on-off keying (OOK) as the predominant modulation scheme. OOK is the most basic form of amplitude shift keying (ASK), in which an amplitude change signifies a change in symbol. In systems using OOK, the laser is turned on to signify a binary '1' and off to signify a '0'. Directly modulating a semiconductor laser is achieved by changing the driving current which produces a change in the carrier concentrations; this is opposed to external modulation where a device modulates the carrier signal after the light has left the device. The change in carrier concentration creates a subsequent change in the optical gain of the laser cavity, turning the laser from off to on. As the carrier concentration changes, there is a change in the index of refraction. The phase of the laser changes as a result of dependency on the index. This change means a phase modulation accompanies a change in amplitude resulting in a frequency shift at the output [14]. The

instantaneous angular frequency can be written as the first derivative of the phase term, containing the gain and carrier concentration dependencies [16]. These relationships can be seen in the following equation [14]:

$$\delta v(t) = \frac{1}{2\pi} \frac{d\phi}{dt} = \frac{\alpha}{4\pi} \left[g(N - N_{tr}) - \frac{1}{\tau_p} \right] \quad (5)$$

This equation shows how the chirp, $\delta v(t)$, is dependent on the change in phase, $d\phi/dt$, which can be referred to as phase modulation. According to (5), this phase modulation is dependent on net stimulated emission rate, $g(N - N_{tr})$, photon lifetime, τ_p , and linewidth enhancement factor, α . For the stimulated emission rate, N is the number of electrons, N_{tr} is the transparency carrier number, and g is a gain coefficient that takes into account the optical confinement factor, group velocity, gain cross section, and volume. The transparency carrier number refers to the point at which there is no net gain or loss due to stimulated emission, meaning the material appears transparent. When a laser pulse is generated, there is an initial transient time in which the amplitude of the pulse is increasing. The result is an optical spectrum that shifts when there is an abrupt change in the laser's amplitude due to the relationship between the index of refraction and carrier density. Limitations such as dispersion and chirp influenced the study of techniques that can mitigate these obstacles; one technique that has been well studied to mitigate these effects is optical injection locking (OIL).

2.2 Optical Injection

Optical injection, as the name implies, entails injecting the light of one laser into the cavity of another. Figure 3 shows a physical interpretation of optical injection. While the full process may be carried out in a variety of ways, the two major components of interest are referred to as the master and slave lasers. The slave laser receives injected light from the master laser, causing a change in the field of the slave laser. By changing the frequency and strength of the injected laser, a variety of different effects can be achieved.

The various effects of optical injection locking have been studied on an assortment of different lasers. The focus of this manuscript will be on the injection of Fabry–Perot semiconductor lasers. These devices use a Fabry–Perot resonator surrounding the gain medium to act as a feedback mechanism necessary for operation. In a semiconductor device, the cleaved facets of the laser provide this reflectivity needed to achieve lasing. Because they are relatively simple in design and relatively inexpensive compared to other lasers available on the market (distributed feedback and cleaved coupled cavity feedback design architectures for example), it is easy to advocate the implementation of Fabry–Perot lasers in the optical logic and wavelength conversion schemes described throughout this document.

Setting aside the cost and/or benefits of Fabry–Perot devices, the multi-mode nature of a Fabry–Perot resonator is what allows for wavelength conversion and other logical operations. Photons resonating in a Fabry–Perot device propagate at various longitudinal modes. The spacing between longitudinal modes is determined by the following equation (6) [17]:

$$\Delta v_L = \frac{c_0}{2nL} \quad (6)$$

Since the gain spectrum covers a large optical span, several of these modes will experience optical gain and be transmitted at the output. Figure 5 illustrates how the gain spectrum encompasses the resonant modes.

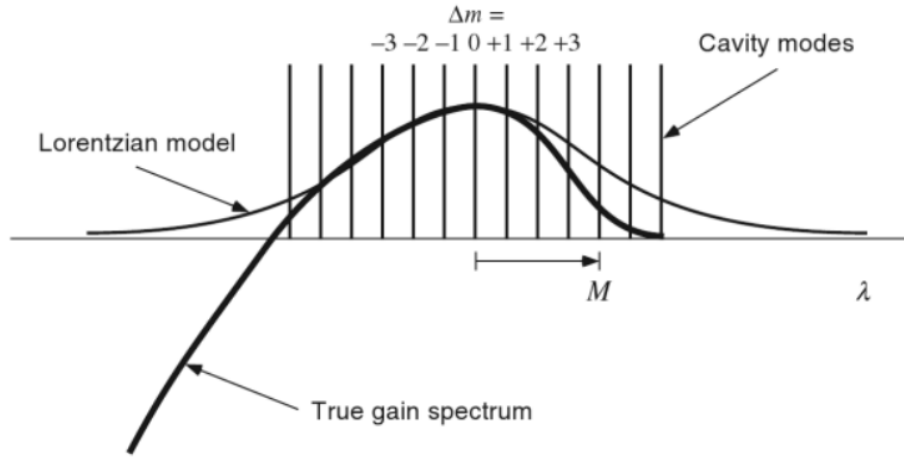


Figure 5: Cavity modes of a Fabry–Perot resonator superimposed over the gain spectrum/Lorentzian model estimate [18].

It is important to define commonly used terms before examining the effects of injection locking. The detuning frequency, $\Delta\omega_{inj}$, is defined as the frequency difference between the master laser, ω_{ML} , and the free-running slave laser, ω_{fr} . Injection ratio, R_{inj} , refers to the ratio of master laser power, P_{inj} , and the free-running slave laser power, P_{fr} . Equations (7) and (8) define the detuning frequency and the injection ratio, respectively [5].

$$\Delta\omega_{inj} \equiv \omega_{ML} - \omega_{fr} \quad (7)$$

$$R_{inj} \equiv \frac{P_{inj}}{P_{fr}} \equiv \frac{S_{inj}}{S_{fr}} \quad (8)$$

Equation (8) shows the injection ratio expressed in terms of the injection photon number, S_{inj} , and free-running slave photon number, S_{fr} .

2.2.1 Injection Stabilities and Dynamics

A laser undergoing optical injection can fall into several categories of operation: stable injection locking, period-one dynamics, period-doubling dynamics, period-quadrupling dynamics, four-wave mixing, multi-wave mixing, and chaos [19]. **Figure 6** shows a map of these different regions of injection dynamics as a function of the normalized injection parameter (ξ) and detuning frequency (f). It is apparent from **Figure 6** that the detuning frequency and injection ratio have significant effects on optical injection behavior. For clarification, the injection parameter, ξ , used in this map is a normalization of the injection ratio equal to $|\eta A_i / \gamma_c A_0|$, with η being the coupling parameter, γ_c as the photon decay rate of the cavity, and A_i / A_0 is the ratio of injected amplitude to free-running slave amplitude.

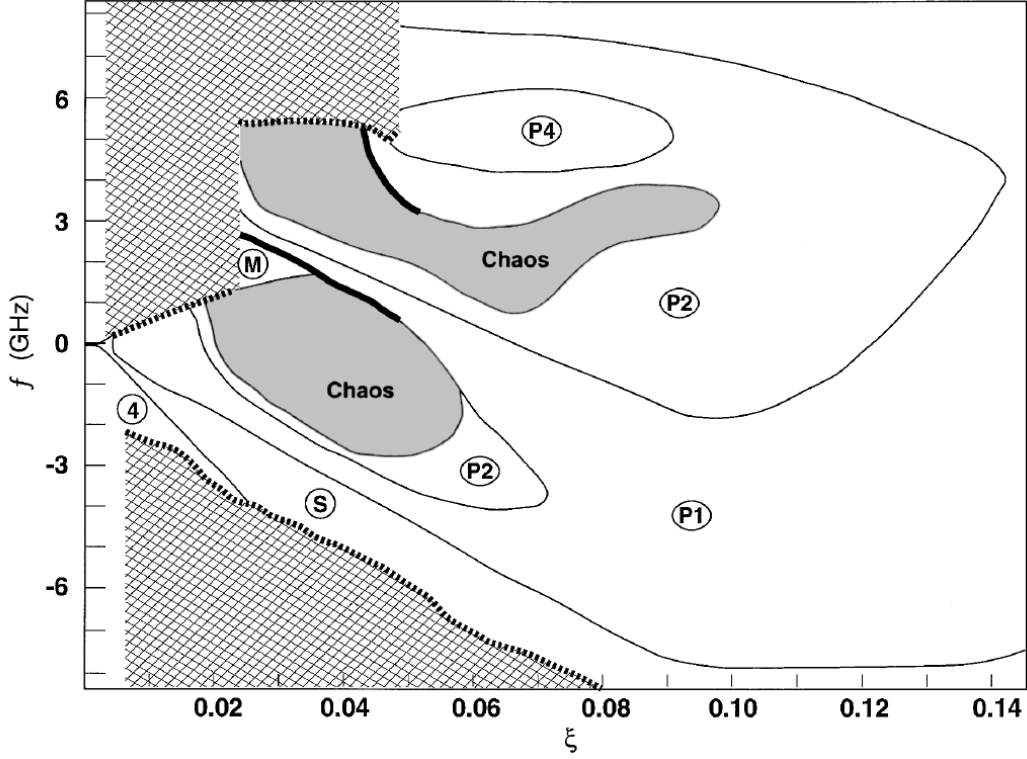


Figure 6: Experimentally obtained map of observed optical injection states in relation to the detuning frequency, f , and normalized injection parameter, ξ . States labeled are: (S) stable, (P1) period one, (P2) period doubling, (P4) period quadrupling, (4) four wave mixing, (M) multi-wave mixing, and chaos (shaded regions) [19].

Although this thesis concentrates on the analysis and effects of stable injection locking, the other dynamic regions have useful characteristics. The period-one dynamical state is predominantly used to generate optical microwave signals [20, 21]. As the detuning frequency and the injection parameters of the laser are adjusted away from the stable region, side modes located away from the injected frequency, ω_{inj} , are amplified [19]. These side modes are separated by the slave laser's relaxation resonance frequency. When these frequencies are generated, a beating occurs creating a widely tunable microwave frequency at the output. The beating of the laser is

referred to as the period-one oscillation frequency. This form of signal generation is quite appealing considering there is no need for much of the complex microwave electronics usually needed. Use of this period-one dynamical state has contributed to a variety of other applications such as radio-over-fiber subcarrier transmissions, AM-to-FM conversions, wavelength conversions, and remote Lidar detection [22, 23].

The chaotic regime has also become a topic of interest in current years. A current area of research concerns the use of optically injected signals in the generation of large broadband random signals [24]. Optically injected lasers can be used as a random signal generator that is high-frequency, but operate at high amplitude, unlike many random signal sources. Under optical injection, experiments performed by Uchida et al. describe the generation of a 20-GHz random signal that is 15 dB above the noise floor [24]. Others have experimented with using chaotic optical injection as a tool in chaotic communication systems. Another analysis performed by Uchida et al. showed that modulation can be performed on a chaotic carrier signal, via a technique known as chaotic masking [25]. In this instance, a chaotic signal is generated and transmitted with a message modulated onto the waveform. This form of chaotic filtering shows that optical injection that is not stably-locked can still be deemed useful.

2.2.2 Rate Equations

When analyzing optical injection locking, initial analysis should begin with the rate equations describing the time-dependent operation of electrically pumped semiconductor lasers. With an understanding of the rate equations, the modifications

to the overall damping rate and resonance frequency of the injected laser can be theoretically predicted, along with stability boundaries for the various dynamic regions introduced in **Figure 6**. Before looking at the rate equations for an optically injected laser, it is important to present the equations for a solitary (free-running) semiconductor laser [14, 18]. The differential equations in Equations (9) and (10) describe the time-dependant changes to the photon ($S(t)$) and carrier ($N(t)$), respectively. Each term in the differential equations describes a mechanism resulting in the generation and/or decay of photons and carriers in the optical cavity.

$$\frac{dS(t)}{dt} = \{g[N(t) - N_{tr}] - \gamma_p\} S(t) + R_{sp} \quad (9)$$

$$\frac{dN(t)}{dt} = J(t) - \gamma_N N(t) - g[N(t) - N_{tr}] S(t) \quad (10)$$

Equation (9) describes the changes in the photon number of the cavity. According to this equation, the photon number is governed by the spontaneous emission rate, stimulated emission rate, and the photon lifetime. The spontaneous emission rate is expressed by R_{sp} and when used to describe the photon number, can generally be ignored to simplify later calculations [14]. The $\gamma_p S(t)$ term in Equation (9) describes the loss of photons in the cavity. The term, γ_p , is the photon decay rate; this is the inverse of the photon lifetime, τ_p , found in (5). The stimulated emission term, $g[N(t) - N_{tr}]S(t)$, depicts the number of photons generated by stimulated emission. The rate of electrons added and removed from the cavity is shown in (10). Injected current density, $J(t)$, accounts for electrons flowing into the cavity. Recombinations of electrons, either spontaneously or through stimulated emission,

account for carriers being removed from the system. The carrier recombination rate, γ_N , takes into account the spontaneous and non-radiative recombinations that take place in the system, such as auger recombination [18, 26]. The net stimulated emission term appears once again, but is subtracted to indicate that stimulated emission is removing carriers from the system.

Using the established rate equations given in Equations (9) and (10), modifications can be made to describe a system where an external field is being injected into the cavity. The following equations describe the standard OIL rate equations [5]:

$$\frac{dS(t)}{dt} = \{g[N(t) - N_{tr}] - \gamma_P\}S(t) + 2\kappa\sqrt{S_{inj}S(t)} \cos[\phi(t) - \phi_{inj}] \quad (11)$$

$$\frac{dN(t)}{dt} = J(t) - \gamma_N N(t) - g[N(t) - N_{tr}] S(t) \quad (12)$$

Looking at these equations, it is evident that (11) is derived from (9) with some additional terms, while (12) remains the same as (10). Since optical injection does not inject additional carriers, the rate equation for electron flow does not change. OIL introduces an additional equation, (13), describing the change in phase difference, $\phi(t)$, between the master and slave lasers [7].

$$\frac{d\phi(t)}{dt} = \frac{\alpha}{2} \{g[N(t) - N_{tr}] - \gamma_P\} - \kappa \sqrt{\frac{S_{inj}}{S(t)}} \sin[\phi(t) - \phi_{inj}] - \Delta\omega_{inj} \quad (13)$$

This phase equation can be derived by separating the amplitude and phase terms from a complex field expression of the slave laser [7]. The real portions of the equation lead to the photon rate shown in (11) and the complex terms create (13).

The additional terms in (11) and (13) contain important parameters used to describe optical injection. The variable κ is referred to as the coupling rate. This parameter is significant in optical injection since it relates the number of photons outside of the cavity to the photons inside the cavity that are contributing to the injection process.

$$\kappa = \frac{v_g}{2L} \frac{1-r}{\sqrt{r}} = \frac{\omega_0}{2Q_c} \quad (14)$$

Since the coupling rate demonstrates a relationship between the photons inside and outside the cavity, it is logical that the mirror reflectivity, r , is used. Other important factors are the group velocity, v_g , and cavity length, L . The second half of (14) describes the rate in terms of half the cavity bandwidth divided by the coupling quality factor, Q_c .

The rest of the variables represent effects of the amplitude and phase effects on the photon number and phase difference. In (13), an injection ratio appears in the form of $\sqrt{S_{inj}/S(t)}$. The amplitude of the field, A , is proportional to S^2 ; therefore, this term is a ratio of the injected amplitude to the slave-laser amplitude. The term appearing in (11), $\sqrt{S_{inj}S(t)}$, is another representation of the field amplitudes. Converting these equations from photon number to amplitude is more complicated than setting $A = S^2$ and is beyond the scope of this paper. The sinusoidal terms that

appear in both equations describe the effect of the phase difference on the field. It is important to note that (13) includes the detuning frequency term, $\Delta\omega_{inj}$, as well as the linewidth enhancement factor, α .

The frequency response of the system can be determined using the rate equations. First the steady-state solutions must be calculated by setting (11)-(13) equal to zero [5, 6].

$$S_0 = \frac{S_{fr} - (\gamma_N/\gamma_P)\Delta N_0}{1 + (g\Delta N_0/\gamma_P)} \quad (15)$$

$$\phi_0 = \sin^{-1} \left\{ -\frac{\Delta\omega_{inj}}{\kappa\sqrt{1+\alpha^2}} \sqrt{\frac{S_0}{S_{inj}}} \right\} - \tan^{-1} \alpha \quad (16)$$

$$\Delta N_0 = -\frac{2\kappa}{g} \sqrt{\frac{S_{inj}}{S_0}} \cos \phi_0 \quad (17)$$

Solutions (15), (16), and (17) represent the steady-state photon number, steady-state phase, and steady-state carrier number. Variable N_0 is the steady-state carrier number; equation (17) is solved for ΔN_0 , which is equivalent to the difference between the steady-state carrier number and the threshold carrier number. This threshold carrier number is related to the transparency number by $N_{th} = N_{tr} + \gamma_P/g$; the threshold number takes into account the photon lifetime in the cavity as well. In order to simplify notation, $z \equiv \kappa\sqrt{S_{inj}/S_0}$, where S_{fr} is the free-running photon number. The photon number of the free-running slave laser can be found by solving (12) in steady-state and setting ΔN_0 to zero. This yields the following:

$$S_{fr} = \frac{J - \gamma_N N_{th}}{\gamma_P} \quad (18)$$

Using these new steady-state values, a solution to the modulation response can be obtained. Equations (11)-(13) can be linearized and presented in a matrix form.

$$\begin{bmatrix} z \cos \phi_0 + j\omega & 2zS_0 \sin \phi_0 & -gS_0 \\ -z \sin \phi_0 / 2S_0 & z \cos \phi_0 & -\alpha g / 2 \\ \gamma_P - 2z \cos \phi_0 & 0 & \gamma_N + gS_0 \end{bmatrix} \begin{bmatrix} \Delta S \\ \Delta \phi_0 \\ \Delta N \end{bmatrix} = \begin{bmatrix} 0 \\ 0 \\ \Delta J \end{bmatrix} \quad (19)$$

Using Cramer's rule this set of linear equations can be solved for the frequency response shown in (20). This result follows the derivation of the modulation transfer function found in [5], which in turn corresponds to the derivation of the free-running modulation transfer function described by Coldren and Corzine [18]:

$$H(\omega) \approx \frac{(\alpha g z S_0 \sin \phi_0 - g z S_0 \cos \phi_0)}{(j\omega + \omega_P)(j\omega - j\omega_R + \frac{1}{2}\gamma)(j\omega + j\omega_R + \frac{1}{2}\gamma)} \quad (20)$$

Here ω_R and γ are the resonance frequency and the damping, respectively. These terms are analogous to those of a free-running semiconductor laser. The term, ω_P , is the third, real pole of the transfer function. The resonance frequency is also referred to as the relaxation oscillation frequency when discussing the transient behavior of a laser. The relaxation oscillations describe the output fluctuations that occur after electrical and/or optical pumping conditions are abruptly changed in amplitude. The damping term describes how quickly these oscillations relax back to a

steady value. Relaxation oscillation frequency, damping, and ω_P are defined by the following equations, respectively [5].

$$\omega_R^2 \approx gS_0(\gamma_P - 2z \cos \phi_0) + z^2 \sin^2 \phi_0 \quad (21)$$

$$\gamma \approx \gamma_N + gS_0 - g(N_0 - N_{th}) \quad (22)$$

$$\omega_P \approx \left[1 + \frac{\alpha}{\omega_R} (\gamma_P + g\Delta N) \right] gS_0 \quad (23)$$

With all of these characters defined, it is possible to establish the enhancements provided by optical injection locking.

2.2.3 Optical Injection Enhancements

Optical injection provides a variety of enhancements, all of which can be used to improve optical communication capabilities. Lau *et al.* provide a rather comprehensive list of these enhancements, as shown in TABLE 1 [5].

TABLE 1: A list of limitations to directly modulated semiconductor lasers and their respective improvements due to optical injection [5].

Fundamental limits		Benefit from OIL
Laser	Mode partition noise (Fabry–Perot laser)	Single-mode with side-mode suppression
	Relaxation oscillation frequency	Enhanced relaxation oscillation frequency
	Non-linear electron-photon coupling	Reduced nonlinearities
	Amplified spontaneous emission noise	Reduced RIN
	Wavelength chirp (non-zero α parameter)	Reduced chirp
Link	Differential quantum efficiency < 1	Increased link gain
	Double-sideband modulation	Near-single-sideband modulation

The derivation in the previous section describes one of these benefits, the enhanced relaxation oscillation frequency. The most important of the enhancements to focus on for the implementation of all-optical injection-locking-based logic and wavelength conversion is the suppression of the Fabry–Perot side modes.

As described previously, a Fabry–Perot semiconductor laser has a spectral profile which contains several modes when it is lasing. Figure 4 shows the different optical spectrums for a free-running and injection-locked Fabry–Perot laser. For a communication system, these side modes cause interference on the receiving end, since each of these modes exists at a different wavelength. When the multi-mode Fabry–Perot signal is sent through a fiber, dispersion effects in the fiber cause these different modes to separate temporally. This effect means that as two modes propagate through a fiber, they will separate in time and be received as separate

pulses; this occurrence is known as mode partition noise. An important characteristic of OIL is the ability to suppress these side modes so that only a single, narrow-linewidth signal is transmitted. One of the earlier experiments to report side-mode suppression achieved a 30-dB improvement of the center mode relative to noise. The power in the central mode was also increased to 94 percent of that in the total longitudinal modes [27].

While the other enhancements provided by optical injection are certainly useful, the mode suppression of the Fabry–Perot laser is significantly relevant to this research. Optical logic is based on suppressing the modes of the slave laser which are not injected. Therefore, using a single master laser it is possible to create a simple inverter. With the implementation of two master lasers, more complicated logic can be created.

2.3 Wavelength Conversion and Optical Logic

Optical logic operations have been performed using a variety of techniques. The majority of research has explored all-optical logic using semiconductor optical amplifiers (SOA) [28]. SOA-based schemes require that the devices are nearly identical, making these gates expensive and precision dependent [29, 30]. Additionally, SOAs require high bias currents as compared to Fabry–Perot laser diodes. Other schemes involve fiber nonlinearities that take advantage of interferometric properties. These techniques do not require as much power as SOA-based logic but require long loops of fiber making them problematic to integrate and susceptible to mechanical perturbations.

While an inhibitor to implementation in high-data-rate, long-haul communication links, the multi mode nature of Fabry–Perot lasers make them an attractive building block for realizing wavelength conversion/optical logic operations. Coupled with the operational changes observed under optical injection, the optical injection of Fabry–Perot lasers becomes an attractive solution for the implementation of all-optical logic operations. The component-level configuration for injection-locking-based architectures has varied among researchers, but each setup has common elements. Data is modulated on to one or more single-mode master lasers. These master lasers are injected into a Fabry–Perot laser cavity acting as the slave. At the output of the injection, an optical band-pass filter (BPF) is used to select the wavelength upon which the new output signal is transmitted. The differences in technique appear when choosing how the data signal locks and unlocks the slave and whether additional injection with a continuous wave (CW) external beam is used [13].

An examination of current research reveals that there are three general methods of performing logic using injection-locked lasers. The simplest approach is to inject the single-mode laser(s) into one or more modes of the Fabry–Perot device, resulting in mode suppression. The use of a filter to examine the suppressed modes results in the logic signal at the output. The next approach requires the use of an additional injected beam, often referred to as a probe beam, and takes advantage of cavity mode shifting effects induced by optical injection. The third method involves a Fabry–Perot device that operates in a single-mode due to the self-injection locking properties of a special designed external cavity [12]. All three techniques have successfully resulted

in the implementation of all-optical logic, and it is important to understand the advantages and disadvantages each method holds.

2.3.1 **Mode-Suppression-Based Logic**

This method is the most obvious approach of the three and is relatively straightforward to implement due to its simplicity. In this approach, the input data is placed on the master laser which is in turn, injected into the slave cavity. This causes suppression of the non-injected modes. With an optical BPF, one of the suppressed modes can be observed at the output. This results in an inverted signal that is carried on a new wavelength. Relatively little has been published on the use of this method. One of the only investigations into this technique was published by Provost and Frey [31], where an inverting logic gate that could operate up to 150 MHz was experimentally demonstrated. The setup used is described in Figure 7.

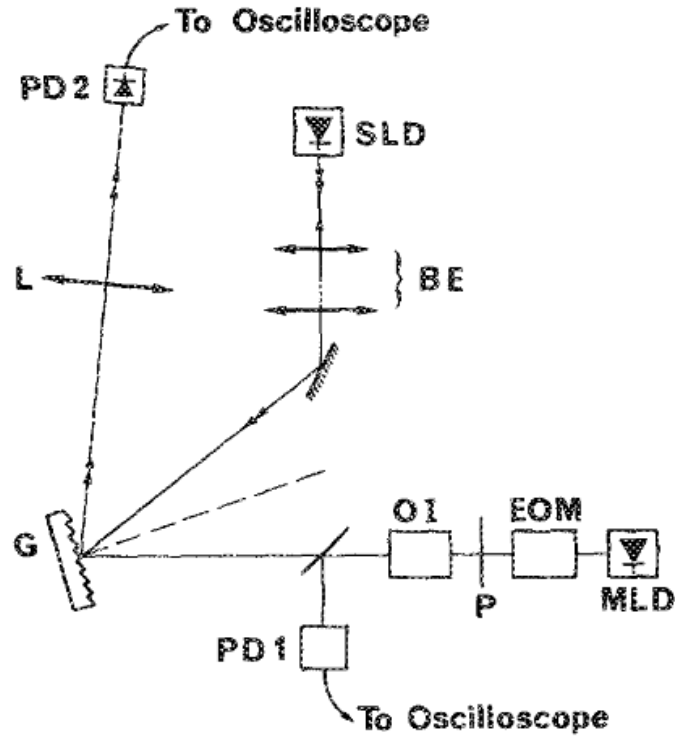


Figure 7: Optical logic inverter. The devices used are labeled as follows; MLD (master laser diode), SLD (slave laser diode), EOM (electro-optic modulator), P (polarizer), OI (optical isolator), G (grating), L (lens), BE (beam expander), and PD1 PD2 (photodiodes) [31].

This setup appears outdated when compared to modern experiments that make use of fiber optics and an optical BPF but it presents the basic setup necessary to create an all-optical logic inverter/wavelength converter. The results showed that there is an approximate 5-ns rise time and a 2-ns fall time in the logical output. This can be seen in Figure 8.

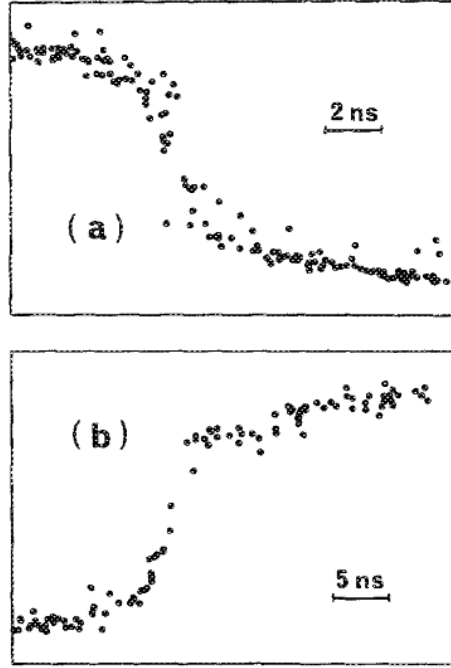


Figure 8: Fall (a) and rise (b) time of the inverted output of the logic gate described in Figure 7 [31].

The inverted output, shown in Figure 8 (a), is falling as the data signal goes ‘high’ and mode suppression is occurring. The rising signal in Figure 8 (b) is the result of the modes unlocking as the data signal turns off. While this apparent asymmetry is not explained fully, it is mentioned that injection locking is more efficient than spontaneous emission. The injection locking and subsequent mode suppression is responsible for the brief high-to-low transition time. The mode unlocking requires spontaneous emission to transition from low-to-high [31]. Apart from this single manuscript, no other researcher into this simplified technique of wavelength conversion and all-optical signal inversion can be found in the literature.

2.3.2 Wavelength Conversion via Mode Shift

A well-known consequence of optical injection is the cavity-mode shift induced in the slave laser cavity. This effect has been used in literature to achieve wavelength conversion and, by extension, other logic functions [13]. To explore this occurrence it is important to highlight the carrier dependence of the light output for an arbitrary mode of a laser. Equation (24) displays the equation determining the longitudinal-mode frequency of a laser output [6].

$$\nu_0 \approx \frac{c_0}{2\mu(N)l} \times m \quad (24)$$

In this equation, ν_0 , l , c_0 , and m describe the output frequency, cavity length, speed of light in a vacuum, and longitudinal mode number. This equation is exactly the same as (6) but here n has been changed to $\mu(N)$; this change indicates the index of refraction μ is dependent on the carrier number, N . As explored, earlier when discussing chirp, this carrier dependence explains the detrimental frequency shifts that occur when directly modulating.

Carrier dependent changes of the refractive index explain the mode comb shifts that occur during the optical injection of a Fabry–Perot laser [32]. The operation can be explained in the following equation [33, 9]:

$$\Delta\omega_{shift} = \frac{\alpha}{2} g(N_0 - N_{th}) \quad (25)$$

Variable $\Delta\omega_{shift}$ describes the frequency shift of the Fabry–Perot cavity modes that occurs upon injection locking. The injection-locking terms α , g , N_0 , and N_{th} , seen previously when analyzing the injection-locking rate equations, are the linewidth enhancement, linear gain coefficient, steady-state carrier density, and threshold carrier density. An important aspect of (25) is the fact that the carrier density must always remain below threshold; therefore, the cavity-mode shift is always negative. Expressed in terms of wavelength, a cavity shift will always be positive. When injection locking occurs, a large portion of the slave laser’s optical power is transferred to the injecting wavelength. The refractive index changes via the linewidth enhancement factor due to the coupling of the index of refraction and carrier density [21, 33, 34]. This causes the red shift seen in (25). This cavity-mode shift is used to explain the enhanced resonance frequency that occurs during optical injection [21, 35, 36]. Equation (26) relates the shift in resonance frequency to cavity-mode shift.

$$\Delta\omega_R = |\Delta\omega_{inj} - \Delta\omega_{shift}| \quad (26)$$

The enhancement to the resonance frequency is not the primary focus of wavelength conversion and logic, but should be noted due to the substantial literature concerning this effect.

Experiments employing a cavity shift utilize what is referred to as a probe beam. This probe beam is a continuous-wave, single-mode beam that is injected into the slave cavity at a different wavelength than that of the master laser transmitting the data. The objective of this method is to use the shift induced by the data signal to

move the cavity modes such that a probe beam falling at a wavelength just inside of the locking range of the selected mode will now fall outside that mode. Figure 9 shows the locking range of a cavity mode and the optical spectra observed at different point in the locking range.

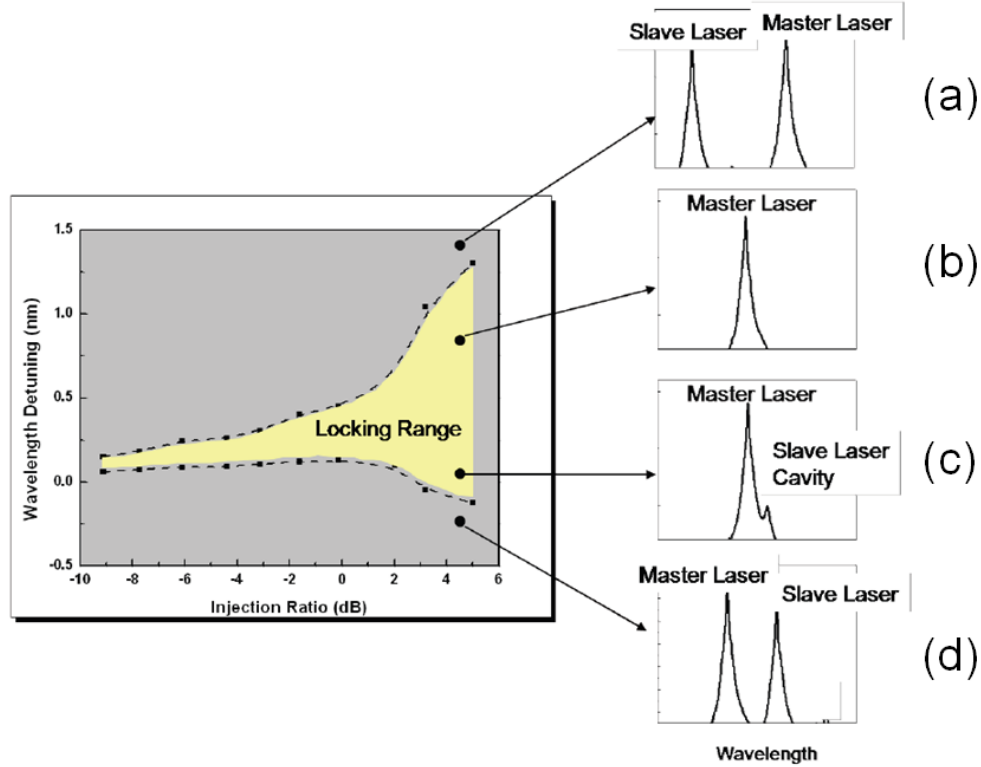


Figure 9: Example locking range of an optically injected laser. (a) Unlocked (b) stably locked (c) locked with the slave mode still present and (d) unlocked [37].

Ideally, inverting logic requires the probe beam be injected in the area described by Figure 9 (c) so that when the locking range is shifted by a positive wavelength it enters the state shown in Figure 9 (d).

Several experiments use the injection of one or more probe beams to achieve wavelength conversion. Hörer and Patzak presented the idea of using the shifting

properties of the injected cavity modes to achieve very fast wavelength conversion as well as logical inversion [13]; Figure 10 describes this process.

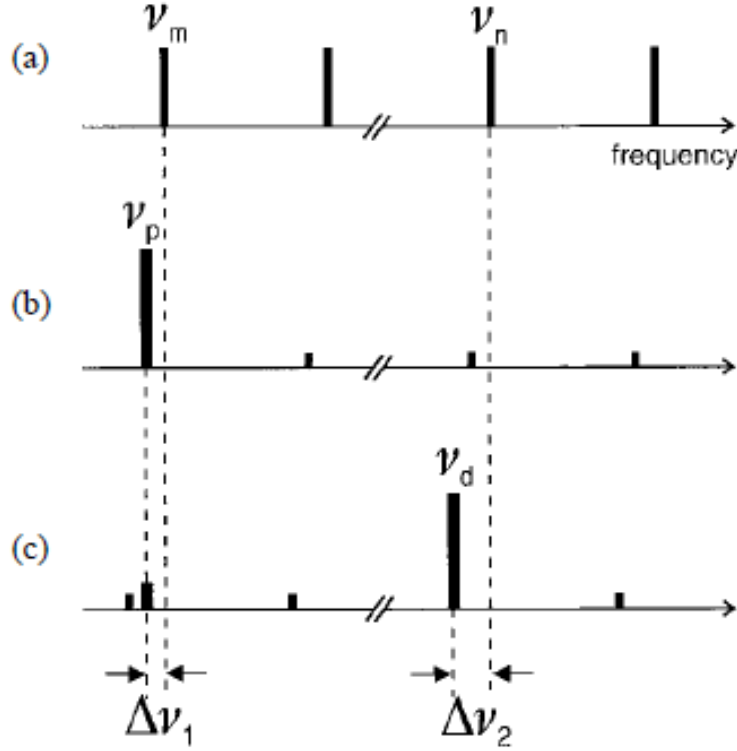


Figure 10: Illustration depicting wavelength conversion using cavity shifting properties with the bars depicting laser modes in the optical spectrum. (a) The free-running slave laser with arbitrary modes, ν_m and ν_n . (b) Injection of probe beam, ν_p . (c) Additional injection of data beam, ν_d , and detuning frequencies, $\Delta\nu_1$ and $\Delta\nu_2$ [13].

This technique begins by injecting a single-mode probe beam into the slave laser, injection locking the slave to that mode. The cavity modes are shifted by detuning frequency of $\Delta\nu_1$ and the laser modes are suppressed with the exception of ν_m [6]. This result can be seen in Figure 10 (b). To achieve wavelength conversion, the data probe is then injected at another mode, ν_n . By injecting the data at an even larger detuning frequency, $\Delta\nu_2$, an even larger red-shift of the cavity modes occurs. This

shift is large enough that the cavity mode being injected by the probe beam moves out of locking range. If a BPF were placed on this mode, the output would observe a logical '0' when the data probe is high; this technique achieves a data inversion and wavelength conversion simultaneously. This procedure can be modified to create a non-inverting output as well. The probe beam is initially injected at a slightly higher frequency than the slave mode so that the probe is outside the locking range of that Fabry–Perot mode. When the data beam injects, the cavity mode's locking range shifts into the probe beam. This causes a '1' to be transmitted at the probe frequency when the data beam is on, resulting in a wavelength/frequency conversion [13].

Numerical analysis performed by Hörer and Patzak measured the degradation of the extinction ratio versus the data rate [13]. Extinction ratio is defined as the ratio of the average power of a logical '1' to that of a logical '0' expressed in decibels. Figure 11 shows the calculated extinction ratio as data rates increase.

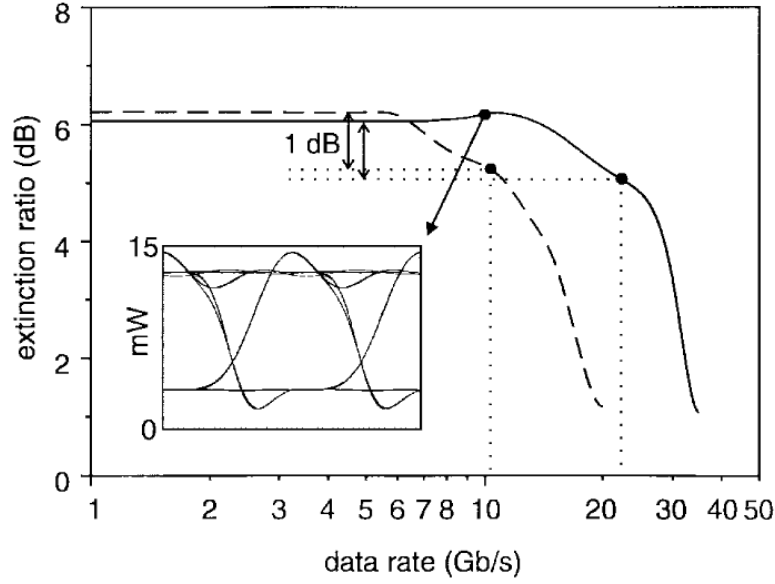


Figure 11: Numerically calculated extinction ratio for wavelength converter based on cavity mode shifting. Dashed line represents the results for a cavity length of 420 μm . Solid line represents cavity mode of 250 μm . The inset eye diagram is calculated for a 250 μm at a data rate of 10 Gbps [13].

Defined as a 1-dB drop in the extinction ratio, the findings suggest that the upper data rate for this method of wavelength conversion is between 10 Gbps and 20 Gbps. A change in the cavity length from 420 μm to 250 μm is responsible for the increase data rate. As the length of the cavity decreases, the photon lifetime decreases. A shorter photon lifetime is responsible for an increase in the relaxation-resonance frequency of the device [13].

Logic gates synthesized using the probe beams rely on the shifting of the slave lasers cavity modes as opposed to the full locking and recovery of the Fabry–Perot modes [13]. This technique of dual-wavelength injection locking has been exploited to achieve a variety of all-optical logic operations. As a reference, TABLE 2 includes the truth tables of the seven standard logic gates.

TABLE 2: List of standard binary logic truth tables.

NOT			
INPUT		OUTPUT	
A		NOT A	
0		1	
1		0	

AND			OR			XOR		
INPUT		OUTPUT	INPUT		OUTPUT	INPUT		OUTPUT
A	B	A AND B	A	B	A OR B	A	B	A XOR B
0	0	0	0	0	0	0	0	0
0	1	0	0	1	1	0	1	1
1	0	0	1	0	1	1	0	1
1	1	1	1	1	1	1	1	0

NAND			NOR			XNOR		
INPUT		OUTPUT	INPUT		OUTPUT	INPUT		OUTPUT
A	B	A NAND B	A	B	A NOR B	A	B	A XNOR B
0	0	1	0	0	1	0	0	1
0	1	1	0	1	0	0	1	0
1	0	1	1	0	0	1	0	0
1	1	0	1	1	0	1	1	1

Use of the probe beam can be expanded on to create more complicated data manipulation schemes. NOR-gate functionality can be achieved following the same principles that create an optical inverter [10]. Two data signals can be used in the same manner as v_d shown in Figure 10. These data signals are detuned in such a way that the cavity modes are shifted out of the locking range of the probe beam when either data signal is on. This functionality can be seen in Figure 12.

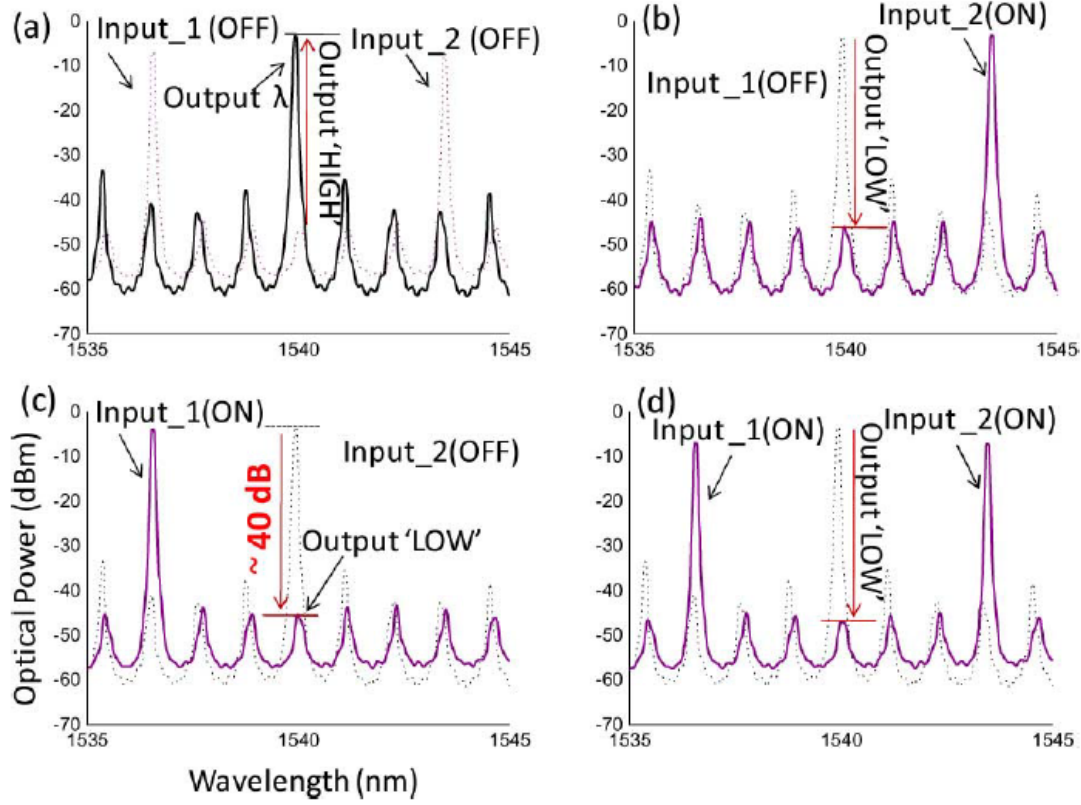


Figure 12: Optical spectrum of an all-optical NOR gate. Grey dotted line represents injection under the probe beam only. (a) No data is injected. (b) and (c) only one data beam is injected. (d) Both data signals are injected [12].

When no signals are injected the output is a '1'. When either data signal (labeled as Input_1 and Input_2) becomes logic '1' the output goes to '0'. Referring to TABLE 2, it is clear that this is a NOR operation. By adding the CW probe beam, the result is a stable performance at 10 Gbps [10]. Others have used this technique for polarization stabilization on pulse widths of 17 ps or over 40 Gbps [38].

Injecting a Fabry–Perot cavity with TM-polarized light creates a different effect than when injection occurs with TE-polarized light [39]. This difference can be observed in Figure 13.

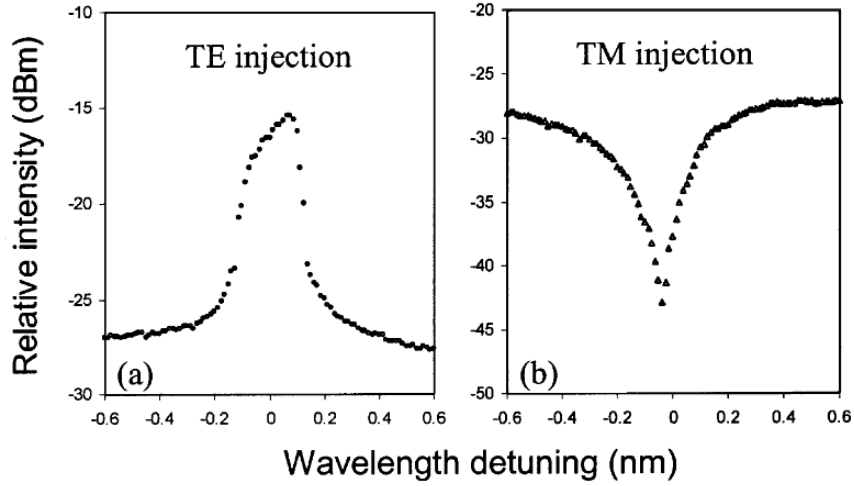


Figure 13: (a) The optical intensity output when injected beam is TE polarized for several detuning frequencies. (b) Output when injected beam is TM polarized [39].

As seen with most of the examples of injection locking discussed thus far, when TE light is injected into a TE Fabry–Perot mode, amplification occurs at the mode in question. When TM light is injected, however, a suppression of the injected beam occurs at the TM Fabry–Perot modes. This absorption effect allows an injection-locked Fabry–Perot laser to be used as an intensity-compensating polarizer as long as the TE and TM modes of the slave are aligned [39].

Additionally, this absorption can be used to achieve wavelength conversion and other logical functions [40, 41, 42, 11]. The principle works the same way as the normal probe beam injection; the TM absorption nulls are shifted in such a way that the TM-polarized probe is suppressed. This process is illustrated in Figure 14.

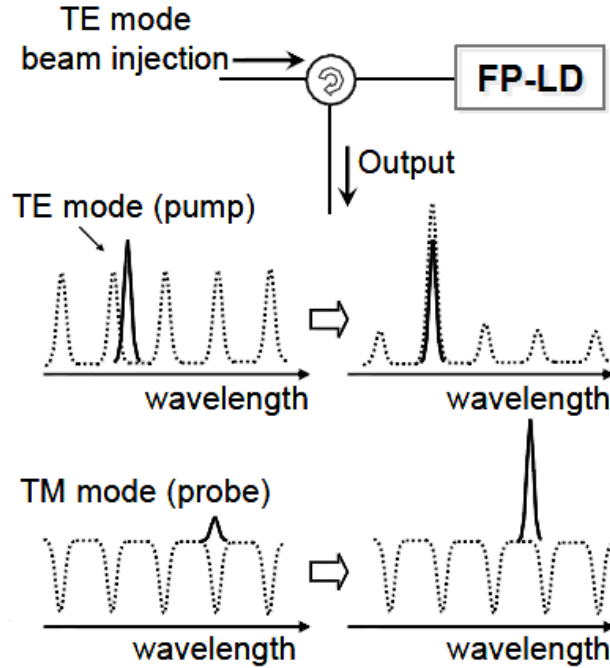


Figure 14: Shift of Fabry–Perot modes by injection of a TE mode and the effects on the TM polarized probe beam [42].

When a TE-polarized data beam is injected, the cavity modes will shift. If a TM-polarized probe beam is injected at one of the TM absorption nulls, the subsequent cavity shift will move the nulls allowing the TM probe to propagate. Using this technique, experiments have demonstrated that data from a single beam can be modulated onto as many as four probe wavelengths simultaneously [42]. Experiments published by Yoo *et al.* have realized NOT, OR, NOR, AND, and NAND logic using a method similar to that shown in Figure 12 but using the suppression of TM-polarized probes [11].

Logic gates using an external probe beam and cavity-mode shifting can be cascaded to achieve higher logical functionality, such as a bit-error monitor [43]. To achieve an all-optical bit-error monitoring system, a NOT gate is constructed and

followed by a NOR gate. In this design if a bit falls between two separate thresholds, the pulse is considered an error bit. The thresholds of the design are determined by the operating conditions of the NOT and NOR gates. The effects of this setup are described in Figure 15.

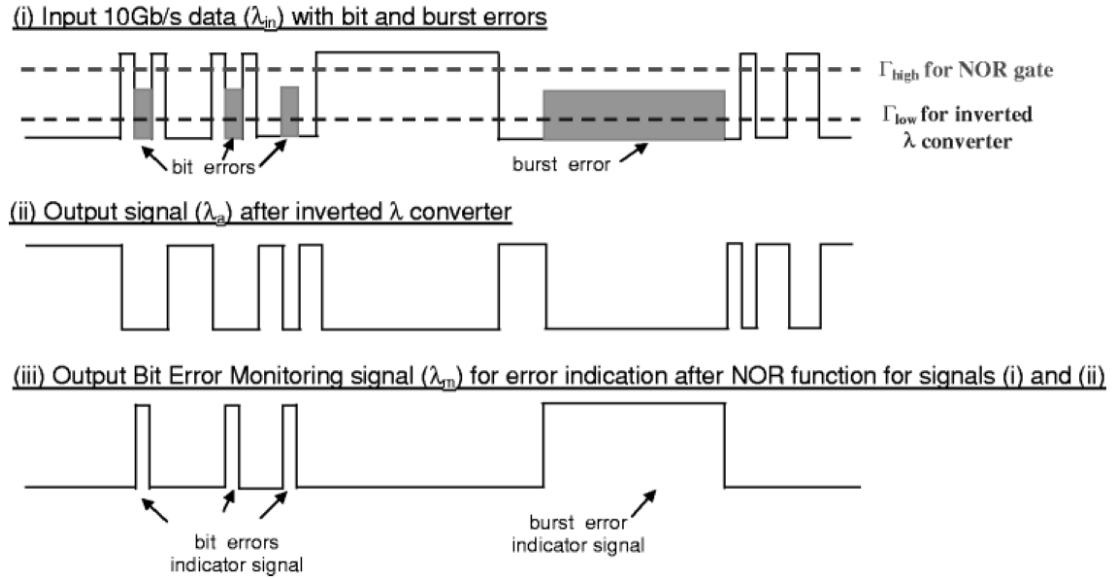


Figure 15: The operation of the all-optical bit error rate monitor. (i) The original signal with errors. (ii) The output of the NOT gate operating with the Γ_{low} threshold. (iii) NOR output of inverted and original signals using the Γ_{high} threshold [43].

The bias current used in the NOT gate slave laser set at such a level that the “error” bits would be enough to injection lock; this creates the signal shown in Figure 15 (ii), where the shaded bits cause a ‘1’ in the inverted output. Using the high threshold, the NOR gate outputs the bits that fell between the high and low thresholds. This error monitoring occurs in real time and results have shown this to be viable at data rates of up to 10 Gbps [43]. Using a similar approach of cascading these simpler gates, more impressive logic functions can be realized.

2.3.3 Single-Mode Fabry–Perot Logic

Logic can be realized using what is referred to as a single-mode Fabry–Perot laser diode (SMFP-LD). This approach is similar to that of the cavity-mode shift method described previously; the slave laser will be operating in a single-mode state when the data beam is injected. The single-mode nature of the slave laser is the result of an external cavity caused by the cleaved end facet of the coupling fiber as opposed to the injection of a separate continuous wave [44]. This external cavity couples the light back into the main laser cavity causing interference similar to injection locking. The cross section of such a device can be seen in Figure 16.

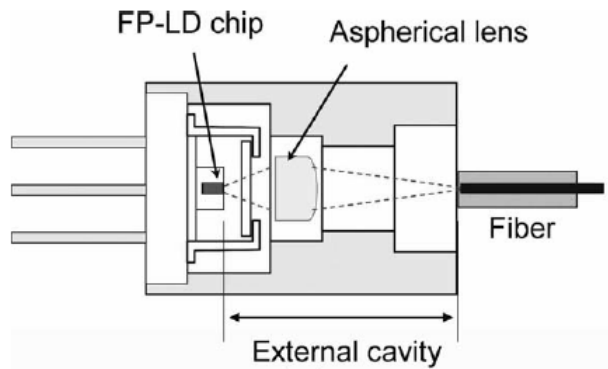


Figure 16: An example of a Fabry–Perot laser diode with an external cavity [44].

A device operating in this manner can be temperature tuned, where a temperature change leads to a change of the refractive index. Changes in the index of refraction cause the optical path length to change, in turn causing the mode spacing of the external cavity to shift. Tuning the longitudinal mode spacing of the external cavity allows the modes of the external cavity to be matched to the longitudinal modes of the Fabry–Perot cavity; this mode alignment causes single-mode operation. The

SMFP-LD presented by Jeong *et al.* achieved a side-mode suppression ratio (SMSR) greater than 27 dB and was tunable across 10 nm [44].

With the Fabry–Perot laser causing its own single-mode state, the CW probe beam used in previous examples of all-optical logic is now unnecessary. With one less laser, a wavelength conversion or logic inversion setup will resemble the simplified approach presented by Provost and Frey with the multi-mode slave replaced by the SMFP-LD [31]. A NOT gate can be achieved using the same cavity-mode shifting characteristics that made the probe beam useful, hence, this approach gives all the benefits of the probe beam with one less laser involved [45]. The injection of light at one of the suppressed side modes of the SMFP-LD causes a red shift of the cavity modes, disturbing the mode matching of the Fabry–Perot cavity with the modes of the external cavity [12]. Much like the probe beam, this method can then incorporate a second master laser acting as a second data signal. By injecting this second data signal at another mode, as was seen in Figure 12, a NOR logic gate can be achieved once again. This method allows for data rates similar to that of the probe beam, 10 Gbps being the data rate achieved by Uddin *et al.* while numerical methods predict this method can achieve up to 20 Gbps [12].

With a manipulation of the master lasers' detuning frequencies and power levels, a NAND gate can also be realized. For the NAND scheme it is necessary that neither data signal is strong enough to cause a cavity shift when injected separately. Only when both data signals are injecting simultaneously are their combined powers significant enough to properly shift the cavity modes and unlock the SMFP-LD slave. A functional all-optical NAND gate realized by Nakarmi *et al.* required a combined

minimum power of -6.17 dBm was needed to suppress the SMFP-LD's dominant lasing mode [46]. If the combined power exceeded -5.02 dBm, the beam of either data source alone would have been enough to suppress the dominant mode. The Fabry–Perot slave used operates with a single dominant mode at 1539.56 nm; the data signals were injected at 1543.08 nm and 1553.04 nm with detuning wavelengths of 0.12 nm and 0.08 nm, respectively.

Once again, these gates can be cascaded and modified to achieve further functionality. All-optical XNOR gates, XOR gates, comparators, flip-flops, and half-adders can be achieved using multiple SMFP-LDs in a variety of configurations [47]. For example, a second SMFP-LD can be injected with the output of the NAND gate described previously. If the output of the NAND gate is tuned in such a way that it suppresses the second SMFP-LD, the inverse of a NAND gate will be received at the output resulting in an all-optical AND gate [48]. Even more complicated is an XNOR gate. The optical spectrum of an XNOR gate can be observed in Figure 17.

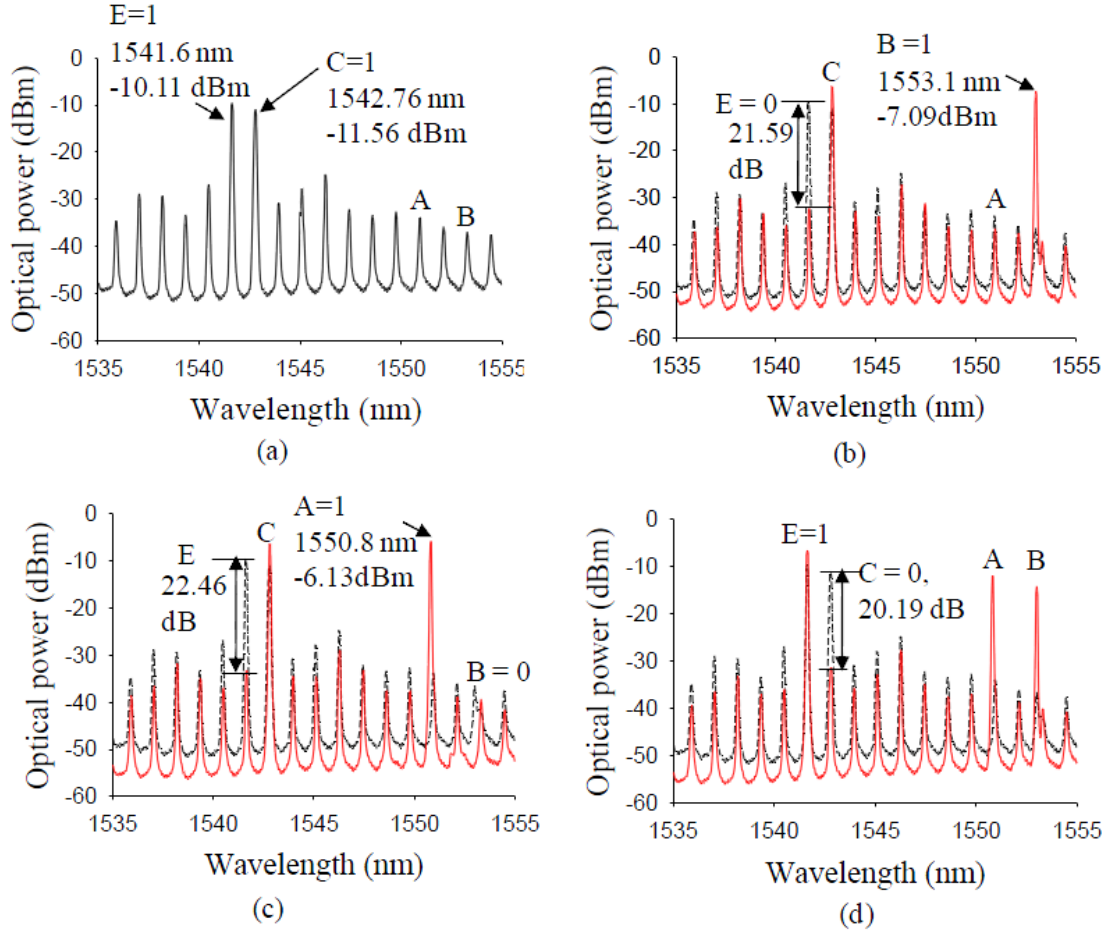


Figure 17: Optical spectrum of XNOR gate. A and B are data signals, C is the NAND output of A and B, and E is the XNOR output of A and B. (a) $A = 0, B = 0, C = 1, E = 1$. (b) $A = 0, B = 1, C = 1, E = 0$. (c) $A = 1, B = 0, C = 1, E = 0$ (d) $A = 1, B = 1, C = 0, E = 1$ [49].

While the XNOR output observed is dependent on the power of data signals A and B, it is also dependent on the power of C, or the output of the NAND. The power of beam C is not enough to suppress the XNOR output, labeled beam E, by itself; when C is injected along with one of the data beams, the power of C and either A or B is enough power to suppress beam E. The power levels and detuning are such that signals A and B are not enough to suppress E without C. The end result is that E will

be suppressed only when one data signal is on [49]. Referring to TABLE 2, this corresponds to an XNOR gate. Once again, this signal can be injected into another SMFP-LD such that the signal is inverted resulting in an XOR [50].

Figure 18 illustrates the functional layouts of the SMFP-LD-based NAND, AND, XNOR, and XOR gates described previously. As shown in this figure, this combination of gates can be cascaded in order to create an all-optical half-adder.

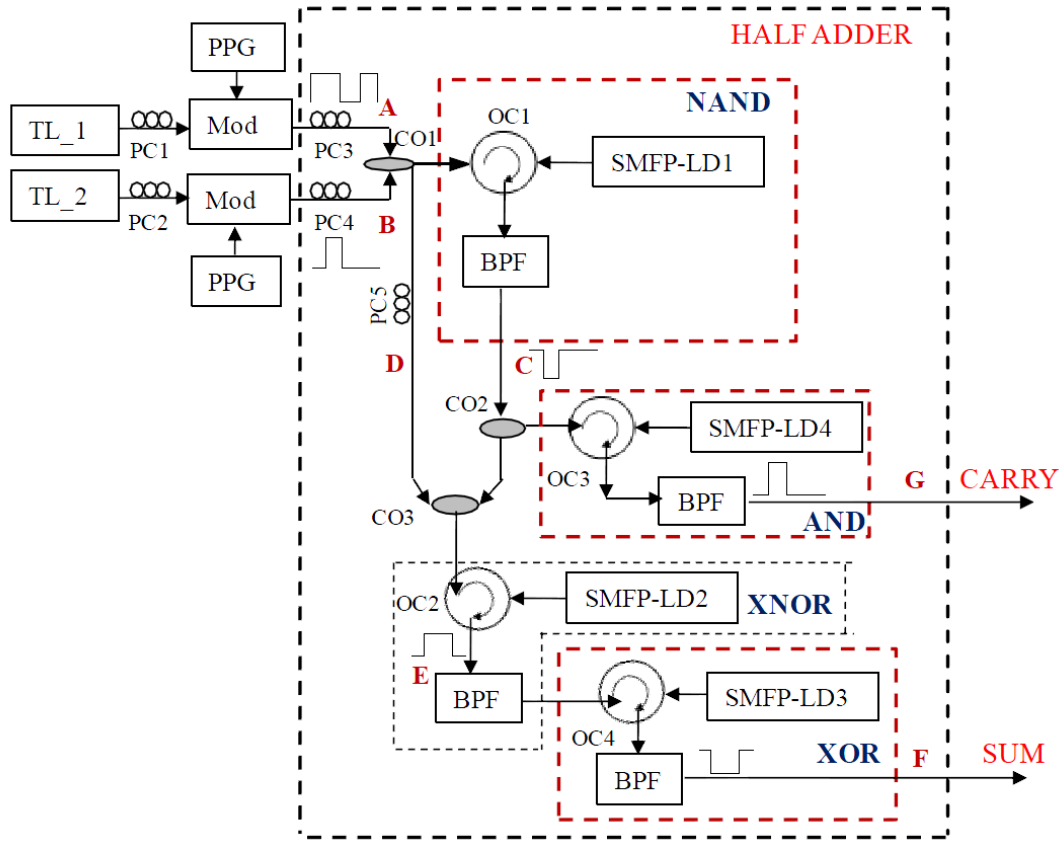


Figure 18: An all-optical half-adder involving all-optical NAND, AND, XNOR, and XOR gates [47].

The all-optical half-adder displays the versatility of SMFP-LD-based logic. Hypothetically, if this logic were to be implemented using the probe-beam methods described earlier, an extra CW source would be needed for each slave laser; the number of lasers needed would increase from six to ten.

2.4 Literature Review Conclusion

Optical communication will be at the forefront of optics research as the capacity needs of society continue to increase. As shown throughout this chapter, the creation of an optical logic gates and wavelength converters requires the integration of many different disciplines. The purpose of this section is to sufficiently describe the theory supporting this research. This chapter provides data from a variety of studies that present theoretical insight relevant to optical logic. With this pertinent background information, it is possible to move forward with an explanation of the methodology used in this research.

3. Methodology

The overarching goal of this research is to create functioning logic gates and wavelength converters using the optical injection-locking technique. This chapter outlines the methodology that is used to conduct this research. One of the intended outcomes of this research is to gather a better understanding of the injection parameters of a multi-mode Fabry–Perot semiconductor laser. Specifically, the injection effects of multiple beams are of particular interest. To achieve a better understanding of the underlying physics, several experiments are performed to analyze the injection locking effects. After performing these experiments, the data are examined using the theories presented in the Literature Review chapter. This research is also compared to experiments performed by Nakarmi *et al.* in which SMFP-LDs were used instead of the multi-mode devices [47]. Additionally, research by Han Liu-Yan *et al.* demonstrated optical logic using a slave laser that required an external probe beam [40]. What differentiates this research from previous efforts is our use of a multi-mode Fabry–Perot laser with no additional external injection.

The beginning of the methodology chapter includes a physical description of the optical logic gates, including an outline of the equipment used. In total, three different logic gates are created: a NOT gate, NOR gate, and a NAND gate. Included with the description of the set up is a detailed description of the individual components used. Once the experiment is constructed and performed, information on the power ratios, detuning frequencies, modulation speeds, and signal quality of the experiment

are recorded. This recorded information will be pertinent to the comparison of the physical operation with the theoretical operation.

3.1 Laboratory Setup

The first stage of this research is to assemble the experimental configuration necessary to study the effects of optical injection. Particular attention was placed on the effects of the injection of multiple master lasers into a single slave, and the dynamics observed when a modulated master laser is injected into a DC biased slave laser. The experimental setups generated required a number of optical components in order to generate, propagate, and record the operational behaviors resulting from the varied configurations. While each of the logic gates is unique, the general set up of these gates is similar. Each gate requires at least one master laser, a slave laser, a band-pass filter (BPF), an external modulator, one or more signal generators, a high-speed oscilloscope, photodetectors, an optical coupler, and various lengths of fiber optic cables. These basic components are needed to create a functioning optical logic gate. In the next several sections, the basic setup required for each of the gates implemented is described.

3.1.1 Wavelength Conversion and NOT Gate

The first gate demonstrated is an all-optical NOT gate, also known as an inverter. This is the same optical circuit used to perform wavelength conversion as well. As the name suggests, the purpose of this logic gate is to invert the signal. The use of a single master laser makes an inverter a simpler experiment than the NOR or NAND gates. Figure 19 illustrates the basic set up of an all-optical NOT gate.

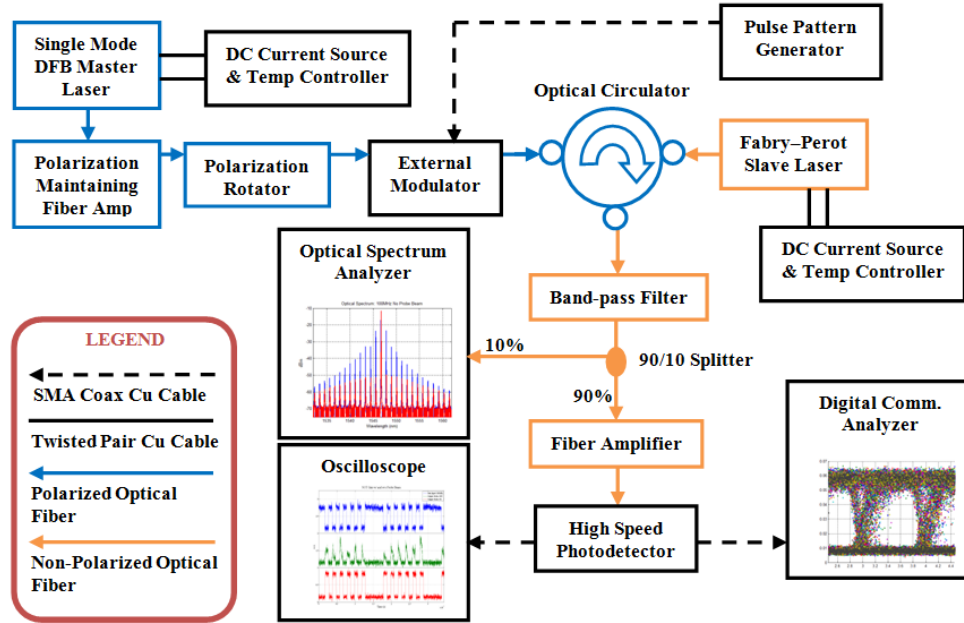


Figure 19: Experimental setup of a wavelength converter/NOT gate dependent on side-mode suppression.

This set up is relatively simple and serves as a starting point for more complicated logic gates that require two master lasers. The DFB master laser generates the single-mode carrier beam that travels by fiber-optic cable to the external modulator. The pulse-pattern generator modulates an ASK signal onto the single-mode carrier beam via the external modulator. Now that the signal is modulated, the single-mode beam is injected into the multi-mode Fabry-Perot laser via the optical circulator. The output of the optical circulator is then sent to an optical BPF. The BPF is tuned to look at the desired output mode of the slave laser. For the NOT gate, the selected modes should be suppressed while injection is occurring at the side modes; when the side mode is not injected, the selected output mode should be propagating. After the BPF, the beam conveys the inverse signal of the master laser and does so at a different carrier wavelength. This signal is converted to an electrical signal via the

high-speed photodiode, after which SubMiniature version A (SMA) cables carry the signals to a high-speed oscilloscope or a digital communications analyzer. A 90/10 optical splitter simultaneously sends the signal to an optical spectrum analyzer as well as the photodetector.

To further study the characteristics of optical logic it would be beneficial to examine the cavity-mode shift approach described in the literature review section. The continuous-wave (CW) probe-beam experimental setup is shown in Figure 20.

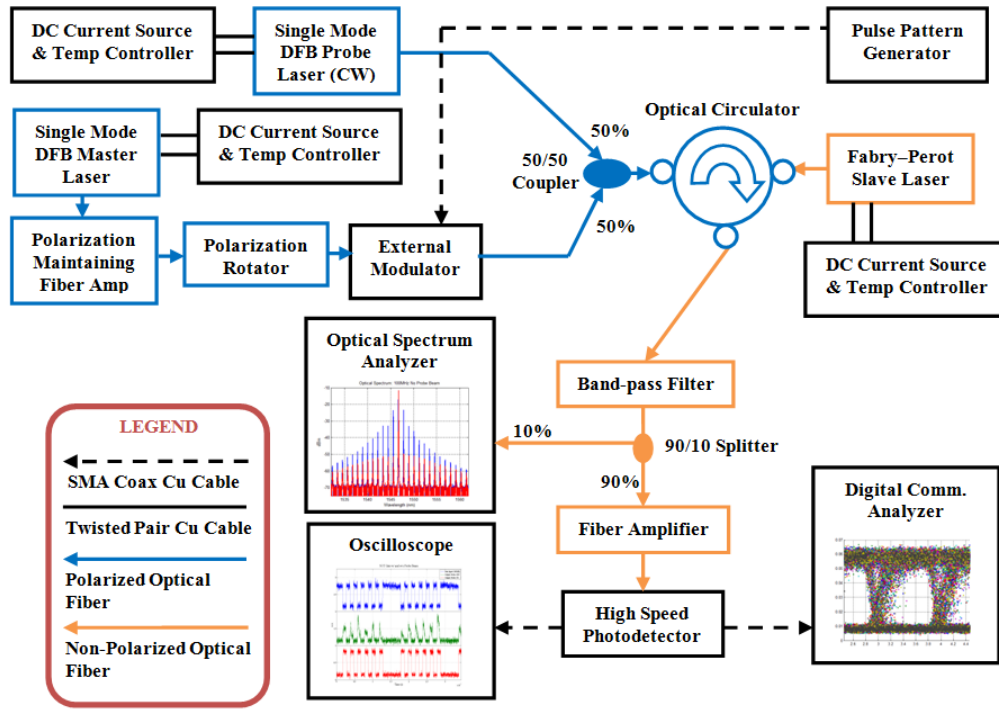


Figure 20: Experimental setup of an all-optical NOT gate/wavelength converter utilizing cavity mode shifting with an external CW probe beam.

The experimental setup of the NOT gate or wavelength converter is similar to that of Figure 19, with the addition of a second single-mode DFB CW laser source. Using a

CW probe beam should enhance the response of an all-optical wavelength converter or NOT gate.

3.1.2 NOR and NAND Gate

Power levels and detuning frequencies differentiate whether the circuit will perform the NOR or NAND gate function. For the NOR gate to operate, the injection of only one of the master lasers must be sufficient to suppress the fundamental mode of the slave laser. This trait means that the fundamental mode will be suppressed when one or both of the lasers are binary high; therefore the fundamental mode will propagate only when the both lasers are binary low. This is the basic functionality of the NOR gate. To demonstrate a NAND logic gate, the power of either laser individually should not suppress the fundamental mode upon injection. Only when both of the lasers are binary high should the fundamental mode be suppressed. One of the fundamental questions of this research is to determine at what point suppression occurs when more than one laser is injected.

Similar to the NOT gate, this circuit can be implemented using the probe beam technique described in the literature review section. The optical circuit tested in this paper can be seen in Figure 21.

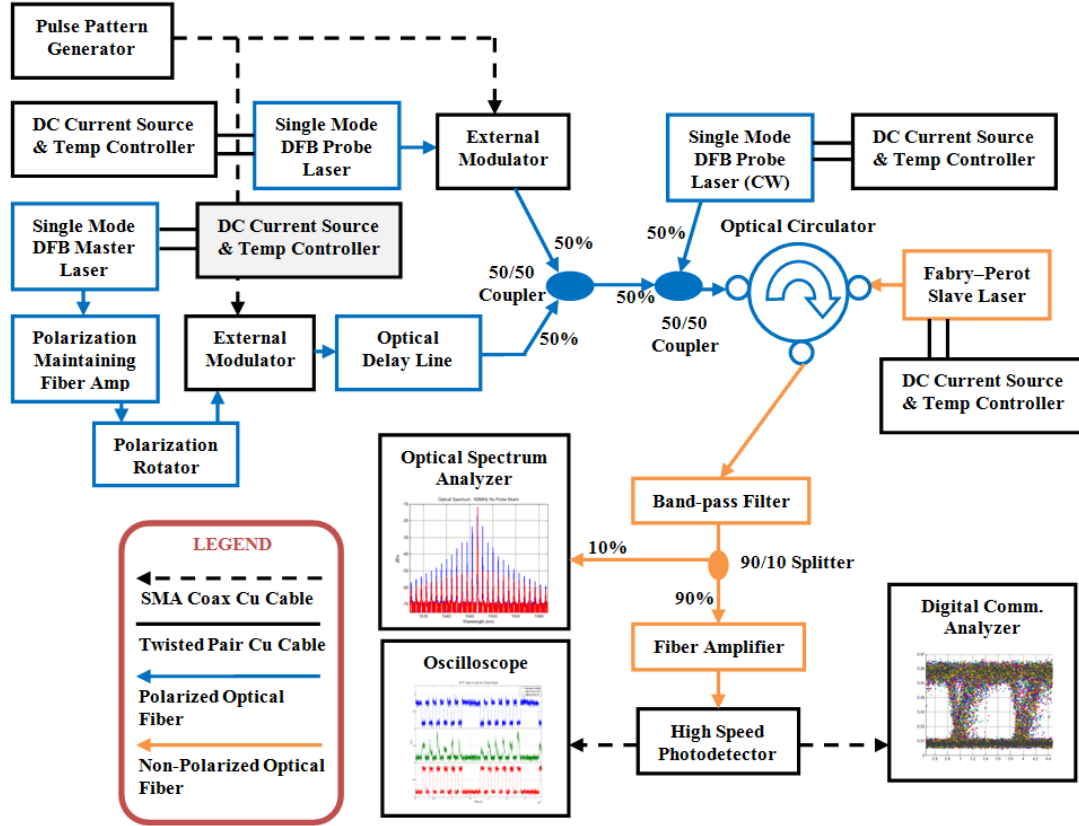


Figure 21: Experimental setup of an all-optical NOR/NAND gate utilizing an external CW probe beam.

The probe beam, as described in the literature review, changes the operation of the all-optical logic by utilizing the cavity-mode shifting properties of an injection-locked Fabry-Perot laser. When testing a logic gate such as the one shown in Figure 21, it is necessary to generate two separate signals so that all possible input permutations can be tested. With only one pulse-pattern generator able to achieve 12.5 Gbps data rates available in the laboratory, it was necessary to split the output of the pulse-pattern generator to each external modulator. The illustration in Figure 22 describes the signal generation process in Figure 22.

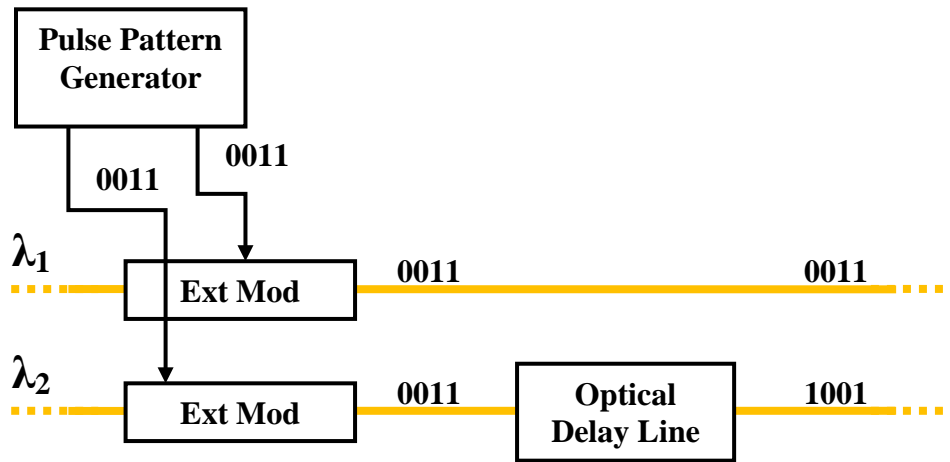


Figure 22: Illustration of signal generation for all-optical logic gates.

By adding an optical delay line along the optical path of one of the lasers, the bit sequence can be aligned so that all four necessary permutations to test the gate can be achieved. Referring to Figure 22, it can be seen that the combinations of outputs that would be received after the optical delay line for arbitrary wavelengths λ_1 and λ_2 would correspond to all the combinations necessary to complete a truth table for a desired logic gate. Using the example of a 12.5-Gbps signal, a one bit delay would correspond to an 80-ps delay. Since the optical delay line is a free-space optical device, it was placed in series with the New Focus tunable laser. The New Focus tunable laser utilizes an optical amplifier at the output that allowing the injected power to be manipulated. Therefore, any power loss caused by this free-space optical device can be compensated for using the amplifier.

Once the two data sequences are generated they are coupled into a single fiber and this data line is then imprinted upon the CW probe beam. With all three wavelengths propagating on one fiber, these signals can now be injected simultaneously into the Fabry–Perot slave laser. After the optical circulator, the

remainder of this circuit is exactly the same as those demonstrated in Figure 19 and Figure 20.

3.2 Experiments

Experiments demonstrated by the previously described laboratory setups are intended to examine the necessary power ratios and detuning wavelengths of the logic gates as well as the speed limitations of these optical circuits.

3.2.1 Mode-Suppression Method

The first experiments are meant to test the laboratory setup shown in Figure 19. The objective of these experiments is to discover the detuning wavelengths and injection strength needed to cause logic inversion and wavelength conversion. After achieving the appropriate settings for this laboratory setup and running the experiment under the optimal settings, it is important to examine the output characteristics associated with the mode suppression. Identifying some key characteristics concerning how mode suppression operates can lead to an analysis of how fast mode suppression can be performed. After examining mode suppression, it is beneficial to examine the improvements provided by the cavity-mode-shift method.

3.2.2 Cavity-Mode-Shift Method

Taking advantage of the cavity-mode-shift should provide a significant increase in the operating speed of the logic gate. For this method, the optical circuit is depicted in Figure 20. The first step of the cavity-mode shift experiments is to determine the proper wavelength detunings and power ratios necessary to make this

method effective. With the cavity-mode-shift method, a CW probe beam is injected at the desired output wavelength, selected using the optical BPF. With this in mind, it is important to examine not only the detuning wavelength and power levels of the data beam but the probe beam as well.

3.2.3 Cavity-Mode-Shift Speed Limitations

With a functioning optical NOT gate and wavelength converter achieved, the next step is to examine the speed limit of the cavity-mode-shift method. This requires a slight modification to the setup shown in Figure 20. The pulse-pattern generator used in the previous experiments is replaced with an HP 83650A Synthesized Sweeper. The synthesized sweeper is capable of generating sinusoidal outputs from 10 MHz to 50 GHz; by replacing the pulse-pattern generator, it will be possible to test the bandwidth limitations of optical-injection-based cavity-mode shifts. For this experiment, the frequency of the sinusoidal input will be increased until the output waveform is no longer recognizable on the measuring equipment used.

3.2.4 NOR/NAND Gate Measurements

The last element to test is the feasibility of all-optical logic using the cavity-mode-shifting properties used to cause wavelength conversion and logic inversion. The laboratory setup illustrated in Figure 21 is constructed to perform these tests. With the detuning and power settings having been fine-tuned by previously described experiments, one laser will remain unchanged while a second DFB laser will be added at another side mode separate from both the first master laser and the fundamental Fabry–Perot mode where the probe beam is injected. To achieve NOR logic, it is

necessary that both injected lasers are capable of achieving an adequate cavity-mode shift independent of the other master laser; additionally, these lasers must achieve a cavity-mode shift when both injected. To achieve NAND logic, neither laser should be capable of properly shifting the cavity modes alone.

3.3 Equipment

These experiments use a variety of specialized optical equipment and high-frequency electrical components; an explanation of these device physics is necessary to understanding the full functionality of the logic gates. Listed in this section are descriptions of some of these devices and how they operate.

The critical components necessary to implement this design include a single-mode external cavity tunable diode laser (New Focus TLB-6300 Velocity Laser-Diode-Controlled laser head) to act as the data signal, a JDS Uniphase external modulator, an Anritsu MP1763C Pulse-Pattern Generator, a fiber-pigtailed quantum-well Fabry–Perot laser diode in a TO-package from Thorlabs mounted in a Thorlabs LM9LD package acting as the slave laser, a polarization-maintaining optical circulator, and a New Focus optical BPF. The external-cavity tunable diode laser was used primarily for convenience and would be replaced with a temperature tunable distributed feedback laser (DFB) laser for application purposes. Secondary components included an SRS LDC501 laser-diode current source to bias the slave laser, a Tektronix TDS 6604 Digital Oscilloscope, an Ando AQ6317B Optical Spectrum Analyzer (OSA), an Agilent Infinium 86100C Digital Communications Analyzer, a New Focus 1444 or 1414 Photodetector, and two Pritel optical amplifiers.

Various fiber-optic splitters, couplers, and fiber-optic cables were used to connect components such that the system output could be observed simultaneously on several measurement systems.

3.3.1 Laboratory Lasers

There are three distinct lasers used in the experimental setups described previously. The fiber-pigtailed quantum-well Fabry–Perot laser diode mentioned prior is used as the slave laser throughout all of these experiments. These experimental setups require several lasers operating simultaneously, each with various temperature, wavelength, or current settings; in order to simplify the variables involved, the Fabry–Perot is set at 20°C with a bias of 20 mA for all experiments performed. This laser has an approximately 300- μm long cavity and operates with the fundamental mode centered at 1546.71 nm for the settings described.

Acting as a probe beam or a data carrying beam, the master lasers used are either the New Focus Tunable laser or JDS Uniphase GaInAsP DFB fiber pigtailed lasers using the SRS LDC501 laser-diode current source. The probe beam laser is a single-mode JDS Uniphase GaInAsP DFB fiber-pigtailed laser which operates at approximately 1550 nm. For these tests the DFB fiber pigtail laser is injected at the fundamental mode of the Fabry–Perot slave laser; the New Focus tunable laser is used to inject the side modes since it has a greater degree of tunability when compared to the temperature controlled distributed feedback laser (DFB) laser. The New Focus external-cavity tunable diode laser was used primarily for convenience and would be replaced with a temperature tunable DFB laser for application purposes. When two

data carrying lasers are needed, as used in Figure 21, the additional laser used is a temperature tuned DFB laser.

3.3.2 Measuring and Analysis Equipment

Measurements of the operational characteristics of the optical logic circuits are performed in both the optical and electrical domains. The primary piece of equipment used to measure the optical characteristics of the experiment is the Ando AQ6317B OSA. As the name suggests, the equipment displays the frequency content of the optical spectrum of the beams propagating along the fibers. The OSA is used primarily to tune the injected single-mode lasers. By observing the optical spectrum of both the Fabry–Perot laser and the single-mode DFB lasers, the detuning wavelengths can be altered and the optical effects of injection locking can be observed.

The electrical signals are observed using the Tektronix TDS 6604 Digital Oscilloscope and the Agilent Infinium 86100C Digital Communications Analyzer. The Tektronix oscilloscope is a real-time oscilloscope and is used primarily to observe the output characteristics of the logic in the time domain while the laser settings are being tuned. The Tektronix oscilloscope is limited by a 6-GHz bandwidth; therefore, it is only useful for examining low data rates (less than 4 Gbps). The digital communications analyzer has a bandwidth greater than 50 GHz therefore it is used for the higher data rate tests.

The communications analyzer is also able to generate an eye diagram and measure waveform characteristics such as jitter and extinction ratio. An eye diagram is a form of data representation commonly used in the communications field to

identify qualitative characteristics concerning a waveform [51]. Eye diagrams are generated by taking an input signal and superimposing several periods of the waveform such that the bit transitions are aligned. A representative eye diagram is shown in Figure 23.

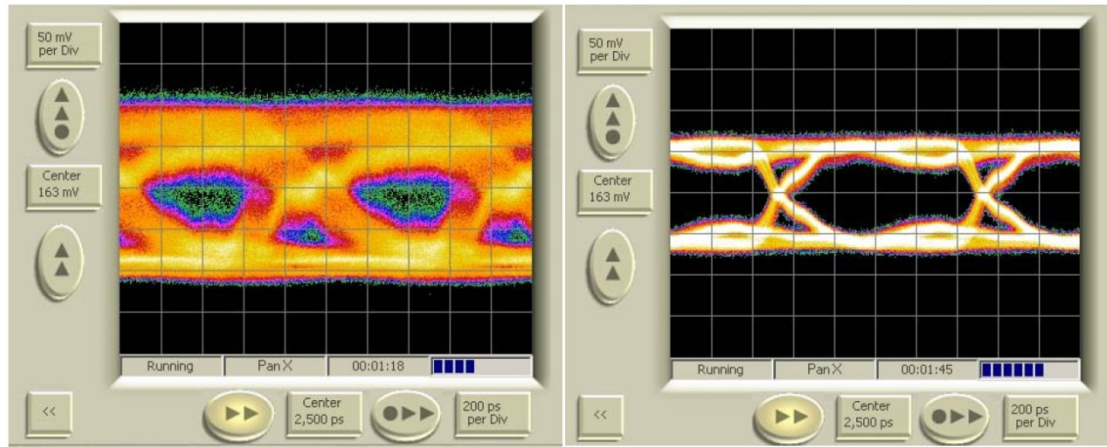


Figure 23: An example of a closed eye diagram (left) and an open eye diagram (right) [8].

Generating this diagram requires a pseudo-random-bit-sequence (PRBS) representative of a “real” data signal, in which the bits do not contain a frequently repeating pattern. This depiction allows for a clear understanding of the high and low logic levels as well as the average transition times. This allows for simple qualitative calculations such as extinction ratio, average power, rise and fall times, jitter, and bit-error ratio (BER).

3.3.3 Mach-Zehnder Modulator

The external modulator used in these experiments is a LiNbO_3 Mach-Zehnder modulator. Mach-Zehnder interferometers are used in interferometry as a measuring

tool; the purpose of this device in these experiments is to superimpose electrical signals onto an optical carrier. A Mach–Zehnder device divides an input beam into two paths. The electrical signal created by the pulse-pattern generator causes a phase change in at least one of the beam paths inside of the modulator. When these beams are recombined at the output, the phase change will subsequently cause either constructive or destructive interference. When using this device, it is important to find the voltage at which the phase is shifted by π [17]. This is the point at which the recombination of the signals should cancel. The optical power output by the modulator was plotted as a function of the voltage bias to obtain its $V\pi$; these results can be seen in Figure 24.

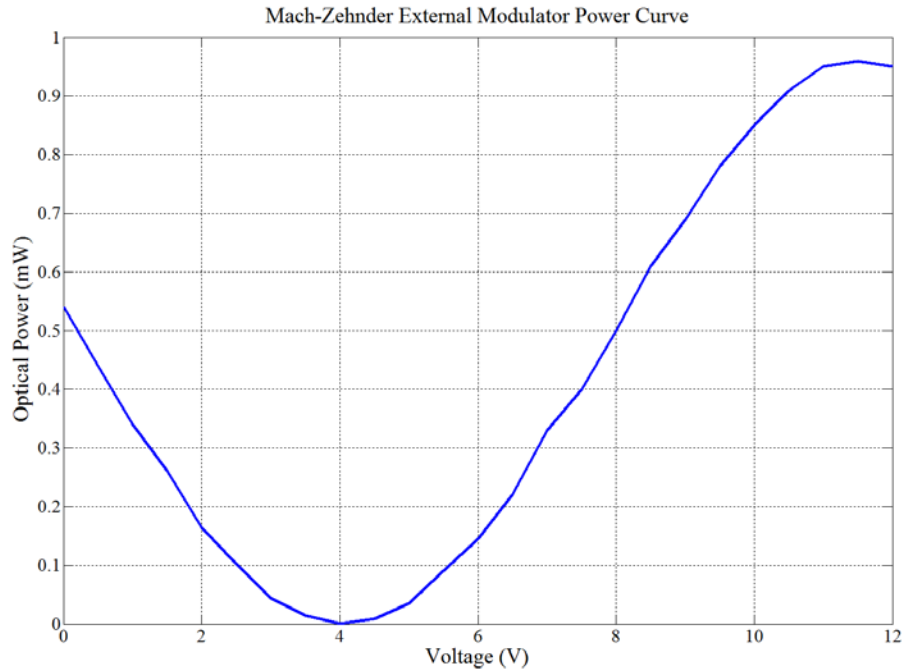


Figure 24: Experimentally obtained measurements of Mach-Zehnder external modulator optical power output versus the DC bias voltage.

An examination of the power output versus the bias voltage reveals the largest change in power will occur when the device is biased at approximately eight volts. By applying an appropriate DC bias voltage to the modulator, the voltage changes from the pulse-pattern generator will cause the phase to shift completely between destructive and constructive interference. In the case of this modulation scheme, the pulse pattern is a square wave, resulting in a square wave at the output. To get a significant change in output power, a voltage swing of approximately 3V peak-to-peak is used in these experiments. This considerable voltage swing requires an RF amplifier be used to amplify the input to the external modulator. The JDSU Mach-Zehnder modulators employed in these experiments have a 20-GHz bandwidth according to the manufacturer.

3.3.4 Optical Circulator

An optical circulator is a device with three ports which takes an input from port one and outputs that beam at port two. Subsequently, inputs into port two are output at port three. For the purpose of this experiment, the master laser goes to port one and exits at port two into the slave laser. This is the point at which optical injection is performed. The injection-locked output signal then propagates back into port two where it is then output at port three. This method of optical injection, referred to by Lau and others as a reflection-style set up, is the most simple to implement with the laser devices we are using [5].

3.4 Methodology Summary

It is the intention of this paper that the results of these experiments will create a better understanding for the power levels and detuning frequencies needed to suppress the modes of a Fabry–Perot laser. The purpose of this chapter is to give a comprehensive explanation of the experiments performed and to ensure the reader has a clear explanation of the equipment being used as well as the actual tests that will be performed to assess these logic schemes. The results of these experiments can now be analyzed in the following chapter.

4. Analysis and Results

The purpose of this chapter is to present and discuss the laboratory results observed during the experimental stage of this thesis. The organization of this chapter follows the sequence of experiments outlined previously in Chapter 3. First, the experimental results of the mode-suppression technique will be presented along with the relevant detuning wavelengths and power levels used to achieve those results. After analyzing the results of the mode suppression technique, the results for the cavity-mode-shift technique involving the addition of the continuous wave (CW) probe beam are explored. With successful results from the cavity-mode-shift method, the next relevant set of data is the result of the cavity-mode-shift bandwidth limitations. Relevant data on the detuning wavelength and power levels needed to achieve the maximum data rate of the cavity-mode-shift experimental setup are included. The last set of results presented is the behavior of the cavity-mode-shift NOR and NAND logic gates.

Before presenting the experimental findings, it is important to define the terms that are used to present the laser settings utilized in the experiments. Due to their prominent use throughout this chapter, (27) and (28) display the detuning wavelength and external injection ratio as defined in this document, respectively.

$$\text{Detuning Wavelength} \equiv \Delta\lambda_{inj} \equiv \lambda_{ML} - \lambda_{fr} \quad (27)$$

$$\text{Injection Ratio} \equiv 10\log_{10}\left(\frac{P_{ML}}{P_{fr}}\right) \quad (28)$$

The OSA readings presented in this chapter show the optical spectrum in wavelength. The corresponding detuning frequencies are also displayed following the detuning wavelengths to give a comprehensive description of the laser parameters. Additionally, the OSA presents the output power of the laser in dBm. The injection ratio defined here is different from the injection ratio defined in (8) as the ratio is expressed in Watts. It also differs from the definition introduced in the *Injection Stabilities and Dynamics* section where it is defined using the injection parameter, ξ , that includes the coupling parameter and the photon decay rate. To further clarify the results, the ratio of $P_{injected}/P_{Free-running}$ will be listed parenthetically following injection ratio measurements. Lastly, the extinction ratio (ER) is used as a qualitative measure of the output signals. Equation (29) shows the definition of the extinction ratio.

$$ER \equiv 10 \log_{10} \left(\frac{P_{avg (logic 1)}}{P_{avg (logic 0)}} \right) \quad (29)$$

The extinction ratio takes the average power of the signal when it is transmitting a logical 1 and the average power of the logical '0'. The ratio of these averaged powers is expressed in decibels [51]. It is desirable to have a high extinction ratio to ensure a sufficient signal-to-noise ratio at the receiver.

Analysis of the results is discussed alongside the findings presented in this chapter. Factors regarding the limitations of the mode suppression, the bandwidth of cavity-mode shifting, and the outputs of the NOR and NAND gates will be discussed. Included in the analysis are any relevant comparisons to experimental or theoretical

results found in previously discussed literature. The first results discussed are that of the mode-suppression method.

4.1 Mode Suppression Results

Mode-suppression-based logic, being the simplest of the designs to implement, was the first of the configurations to be tested. The experimental configuration described by Figure 19 was tested using the Fabry–Perot slave laser set to an operating temperature of 20°C and a biasing current of 20 mA; the data carrying master laser is injected at 1544.61 nm with an injection ratio of -2.269 dB (0.593 times). The optical spectrum of the slave laser with (injection locked) and without (unlocked) injection is shown in Figure 25. The optical BPF window is illustrated to clarify which of the modes is used to convey the logic output.

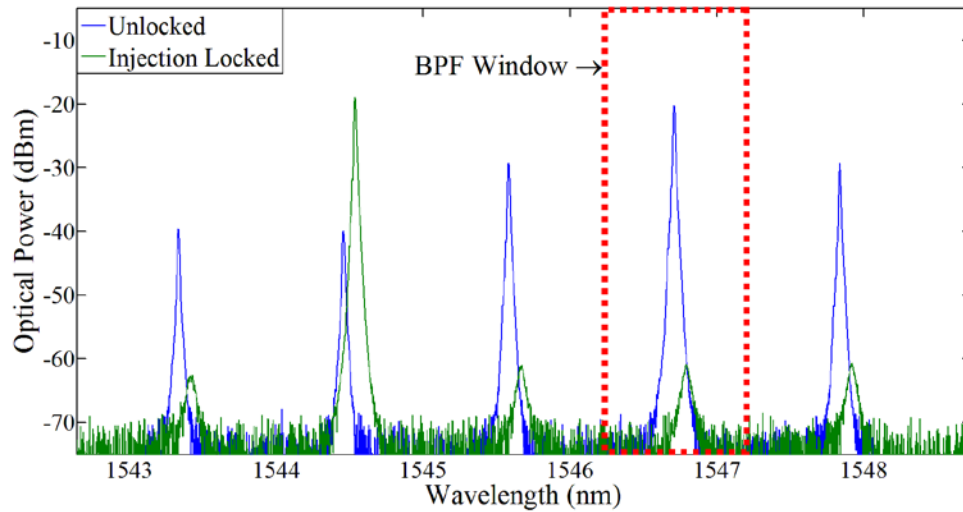


Figure 25: Optical injection with a single-mode DFB into a slave Fabry–Perot cavity causing a suppression of adjacent side modes.

The master laser is injected at an arbitrarily lower wavelength two modes away from the fundamental mode of the slave laser. The wavelength detuning of the master laser at this mode is 0.148 nm (-9.8 GHz), and the free-spectral range of the Fabry–Perot cavity was measured to be 1.12 nm (141.3 GHz). The optical BPF filters the fundamental mode of the Fabry–Perot slave centered at 1546.71 nm (193.96 THz).

Several different pulses were generated to observe the behavior of the logic inverter. Examples of the resulting waveforms generated by this can be observed in Figure 26.

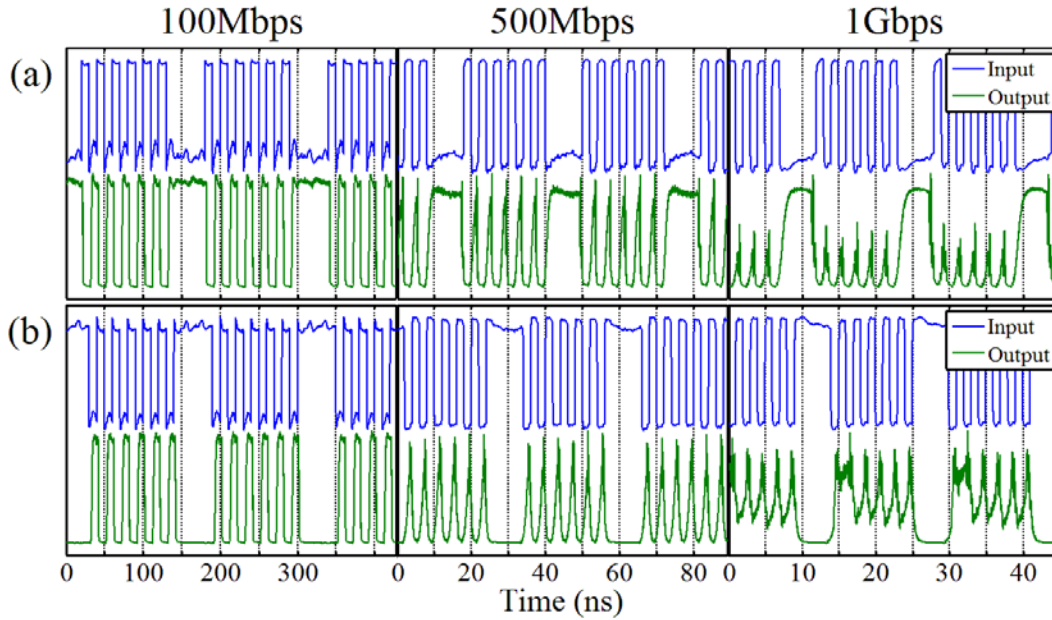


Figure 26: Oscilloscope results for modulation at 100 Mbps, 500 Mbps, and 1 Gbps. The top row (a) of results show a 16 bit input waveform of 0000101010101010. The bottom row (b) uses a pattern of 1111101010101010.

Using two different modulating bit patterns (detailed in Figure 26 (a) and (b)), an asymmetry is observed in the time transient of the mode-suppression response of the Fabry–Perot slave laser. This asymmetry is highly pronounced at the higher data

rates. The first bit sequence contains five consecutive ‘0’ bits, where the master laser is not injecting, followed by a 10-bit pulsed pattern. Observing the 1-Gbps responses to this pattern in Figure 26 it is clear that the gradual rise time of the output signal limits the achievable data rate to below 500 Mbps. The slow rise time prevents the abrupt 1-ns pulses from reaching their full power while the master laser is not injecting. In contrast, the brief fall time that occurs upon injection indicates that the time needed to suppress the modes of the Fabry–Perot is much less than the time needed for the same modes to recover. This is most likely explained by the fact that the recovering modes must first be initiated by spontaneous emission before lasing can begin.

The 1-Gbps response of the second pattern, illustrates another interesting characteristic; as the modes recover from being suppressed from the long sequence of ‘1’s in the input, the slow rise time in the output prevents the device from responding quickly to the subsequent bits. It is not until the carriers are fully recovered that the injection can effectively suppress the modes again. Even though the outputs fall time is sharper than its rise time, it is still not fast enough to reach full suppression during the 1-ns pulses. The asymmetry in the rise and fall time is more pronounced in the eye diagrams displayed in Figure 27.

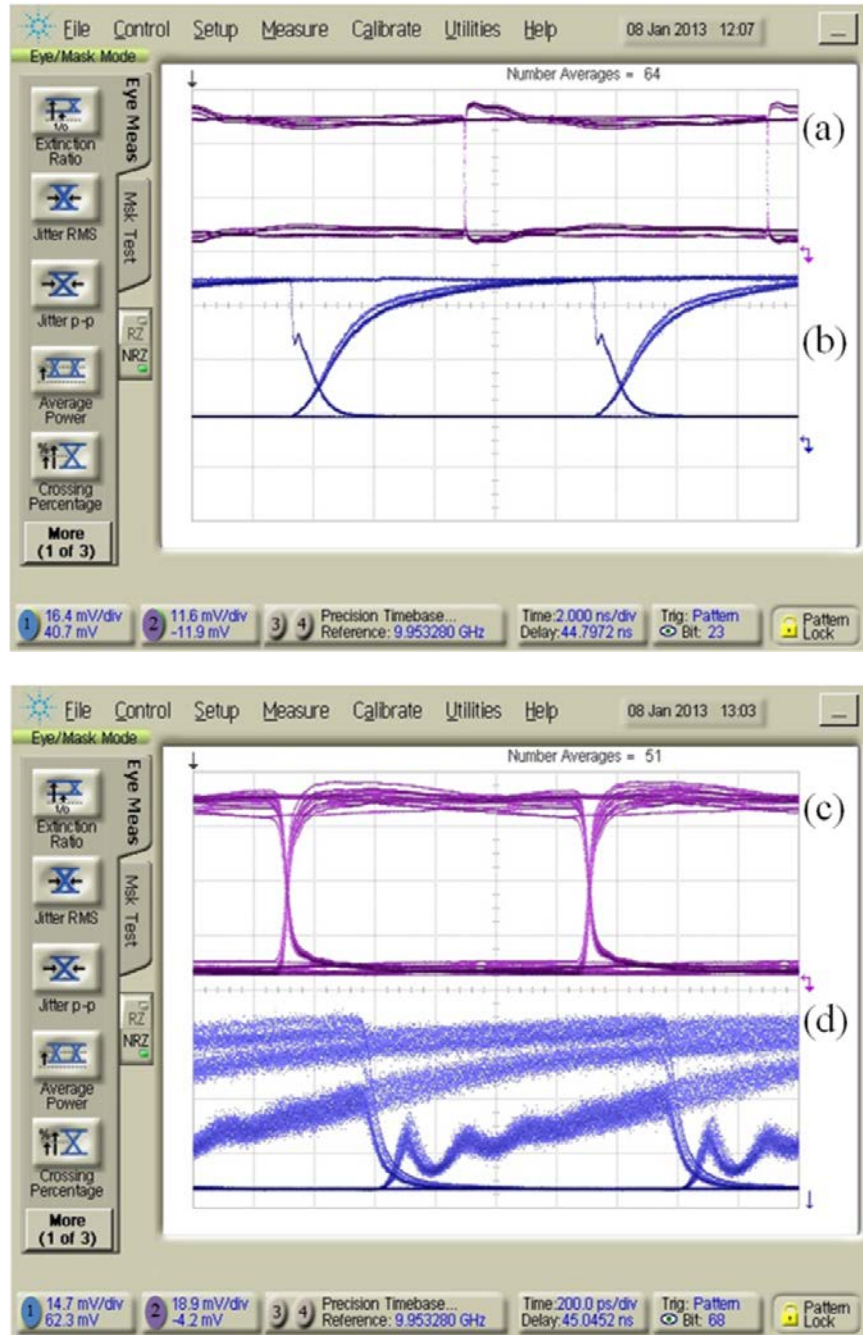


Figure 27: Top eye diagram (a) 100-Mbps PRBS input signal and (b) inverted output signal using mode suppression. Bottom eye diagram (c) 1-Gbps PRBS input signal and (d) inverted output signal using mode suppression.

The extinction ratio for the 100-Mbps can be estimated at about 7.53 dB.

Calculating an accurate and meaningful extinction ratio for the 1-Gbps signal is far

more difficult considering the long rise time. As evidenced by the data, the upper limit of the Fabry–Perot suppression method is below 500 Mbps for error-free transmission. Using the slow rise time of approximately ~1.85 ns as the limiting factor on the signal, the highest modulation rate achievable before signal integrity is lost is approximately 550 Mbps.

Mode-suppression wavelength conversion is the most straightforward approach to wavelength conversion; therefore, it would be desirable if any improvements can be made to this method that do not involve the addition of extra components. One attribute that may provide a bandwidth improvement would be the length of the slave laser cavity. The photon lifetime of a device is closely related to the cavity length according to the following two equations (30) (31) [14, 18]:

$$g_{th} = \alpha_{int} + \frac{1}{2L} \ln \left(\frac{1}{R_1 R_2} \right) = \alpha_{int} + \alpha_{mir} \quad (30)$$

$$\frac{1}{\tau_p} = \Gamma v_g (\alpha_{int} + \alpha_{mir}) = \Gamma v_g g_{th} \quad (31)$$

The amount of gain needed to overcome the cavity losses is referred to as the gain threshold, g_{th} . Total cavity losses are the summation of the mirror losses, α_{mir} , and internal cavity losses, α_{int} . The term describing mirror losses involves the cavity length, L , and mirror reflectivities, R_1 and R_2 since these losses are averaged over the cavity length. Fabry–Perot lasers use cleaved facets meaning the reflectivities are dependent on the refractive index of the semiconductor and cannot be easily altered. The cavity length is the most straightforward device aspect to manipulate. Since the photon lifetime, τ_p , has an inverse relationship with the threshold gain, a decrease in

cavity length increases the gain threshold and subsequently causes a decrease in the photon lifetime. It is possible to derive a formula for the frequency response of a semiconductor laser by performing a similar analysis as that which led to the optical-injection frequency response seen in (20). The 3-dB bandwidth of a device can be ascertained by the following equation [14, 18]:

$$f_{3dB} \approx \left(\frac{3G_N P_b}{4\pi^2 \tau_p} \right)^{1/2} \quad (32)$$

The photon lifetime possesses an inverse relationship with the 3-dB bandwidth; effectively, a decrease in the cavity length decreases the photon lifetime and increases the 3-dB bandwidth of the laser. If one were to assume the modulation of cavity modes could be approximated by the same small-signal analysis as the frequency response of the laser, a reduction in cavity length would improve the speed of a device under this method of operation as well. Hence, the bandwidth limitation found in these experiments is not universal and is most likely improved by a shortening the cavity of the slave device.

4.2 Cavity-Mode-Shifting Results

Next, the injection of a CW probe beam, illustrated in Figure 20, at the desired mode is tested to determine the improvements provided through utilization of the cavity-mode shift occurring under injection locking. For this case, the MMFP-LD laser is kept at the same biasing current and temperature. The master laser is tuned to 1544.64 nm and is amplified to 1.79 dB (1.51 times) compared to the power of the adjacent Fabry–Perot mode. The detuning from this mode is 0.189 nm (-23.77 GHz);

the large detuning and high power ensure the injection will have a more drastic effect on the cavity modes. The probe beam was tuned to 1546.74 nm, a detuning of 0.032 nm (-4.01 GHz), and given an injection ratio of -10.46 dB (0.09 times) with respect to the adjacent mode. This optical spectrum can be observed in Figure 28.

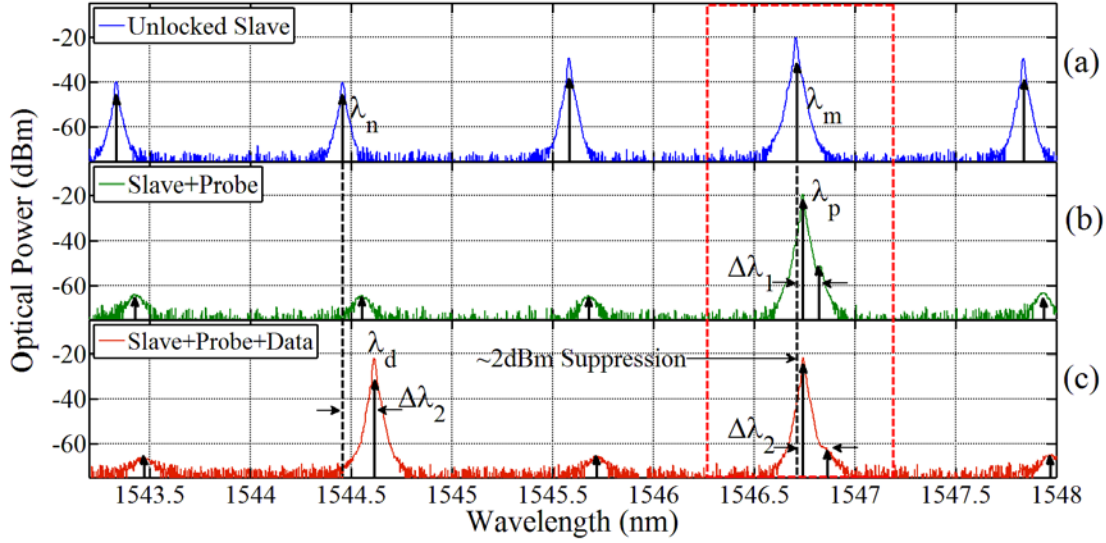


Figure 28: Optical spectrum of an all-optical inverter using a CW probe beam. (a) Optical spectrum of an unlocked MMFP-LD (b) Slave laser under injection from the CW probe only (c) Injection of data signal and probe.

Here λ_n and λ_m are the input and output wavelengths, respectively. Figure 28 (b) shows the injection of probe beam, λ_p , with the subsequent wavelength shift of $\Delta\lambda_1$. The last frame, Figure 28 (c), shows the injection of the data beam, λ_d , inducing a shift of $\Delta\lambda_2$. This shift allows for a suppression of 2 dBm at the output where the probe beam is injected. Simply put, Figure 28 (b) indicates an input of ‘0’ with an output of ‘1’, whereas (c) indicates an input of ‘1’ with an output of ‘0’. With the very weak injection power and shorter detuning wavelength, any shifting of the cavity

modes would be more than enough to unlock the probe beam from its adjacent mode.

Figure 29 shows the results in the time domain.

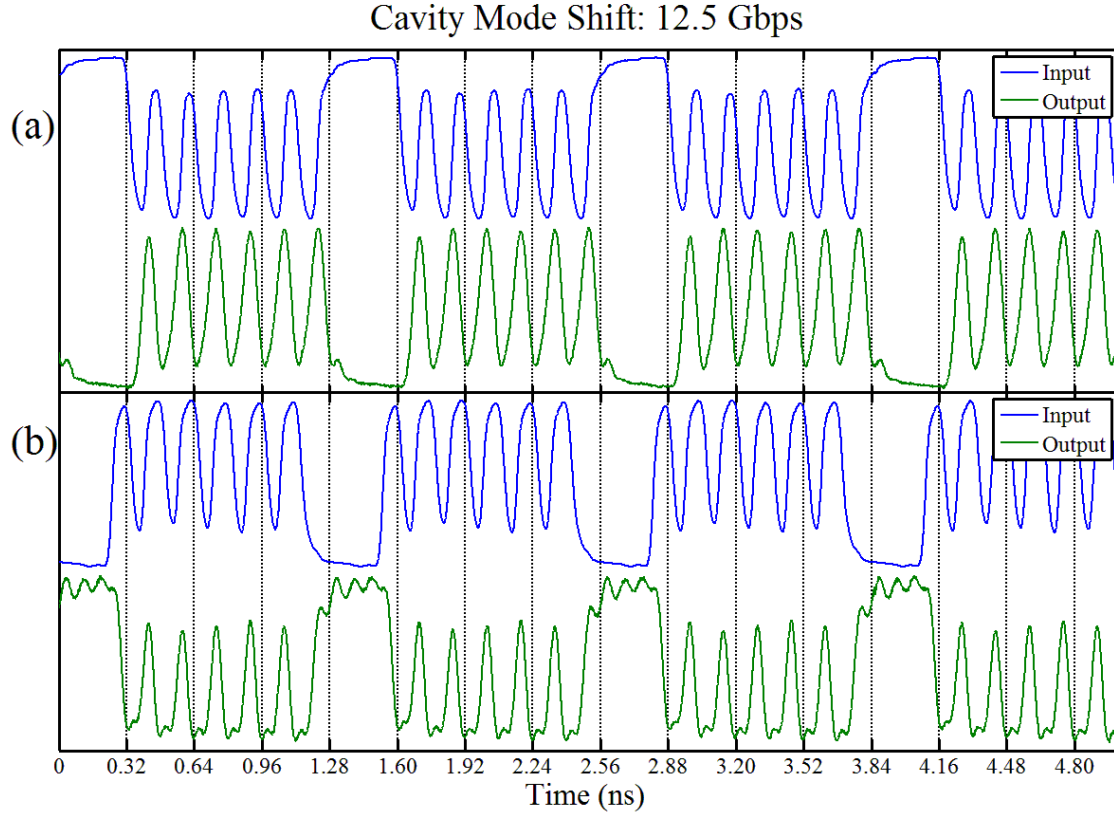


Figure 29: Waveforms generated using the cavity mode shift method. The top row (a) of results show a 16 bit input waveform of 1111010101010101. The bottom row (b) uses a pattern of 0000101010101010.

An eye diagram for an injecting data signal carrying a 12.5-Gbps non-return to zero (NRZ) 2^7-1 pseudo-random-bit-sequence (PRBS) signal is shown in Figure 30.

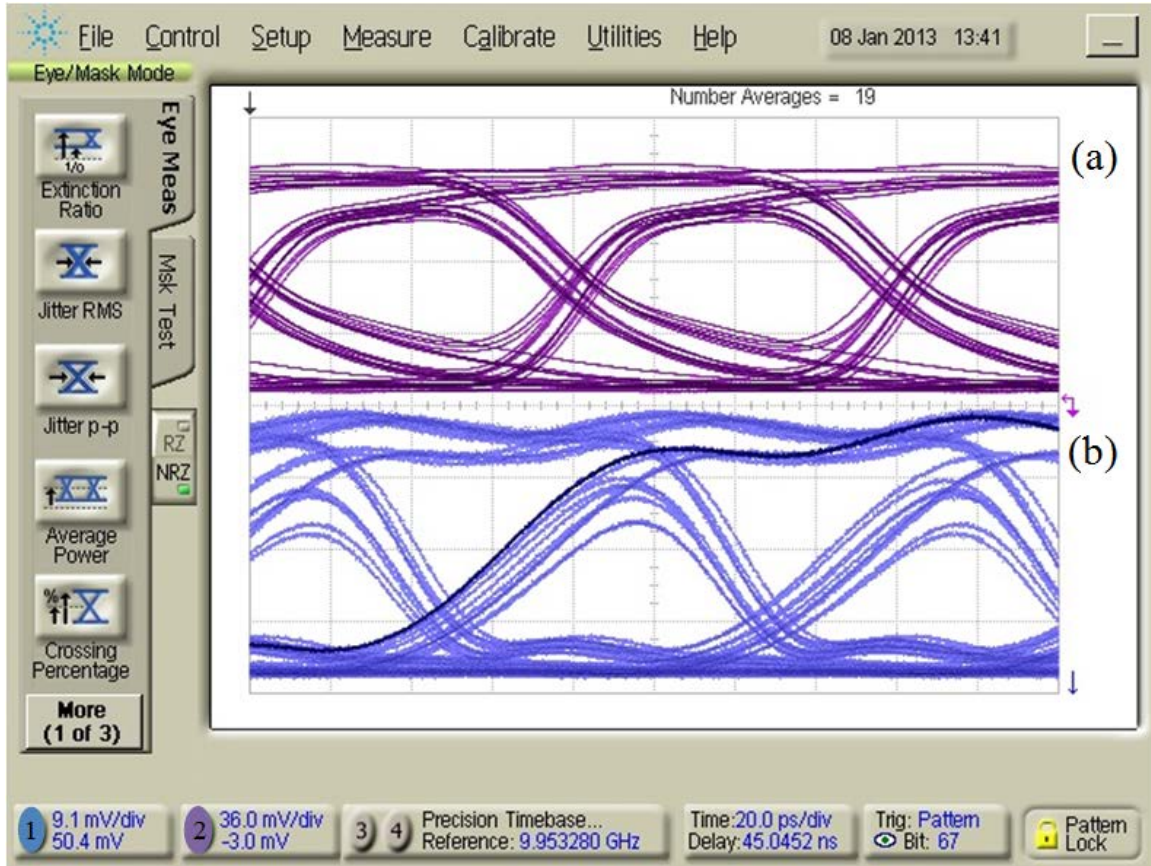


Figure 30: Eye diagram of probe beam (a) 12.5 Gbps PRBS input signal and (b) inverting output signal.

The extinction ratio of the waveform expressed in Figure 30 is approximately 3.59 dB.

The eye diagrams, illustrated in Figure 31, convey the improvements provided by the cavity-mode-shift technique as compared to the mode-suppression method for a 1-Gbps signal.

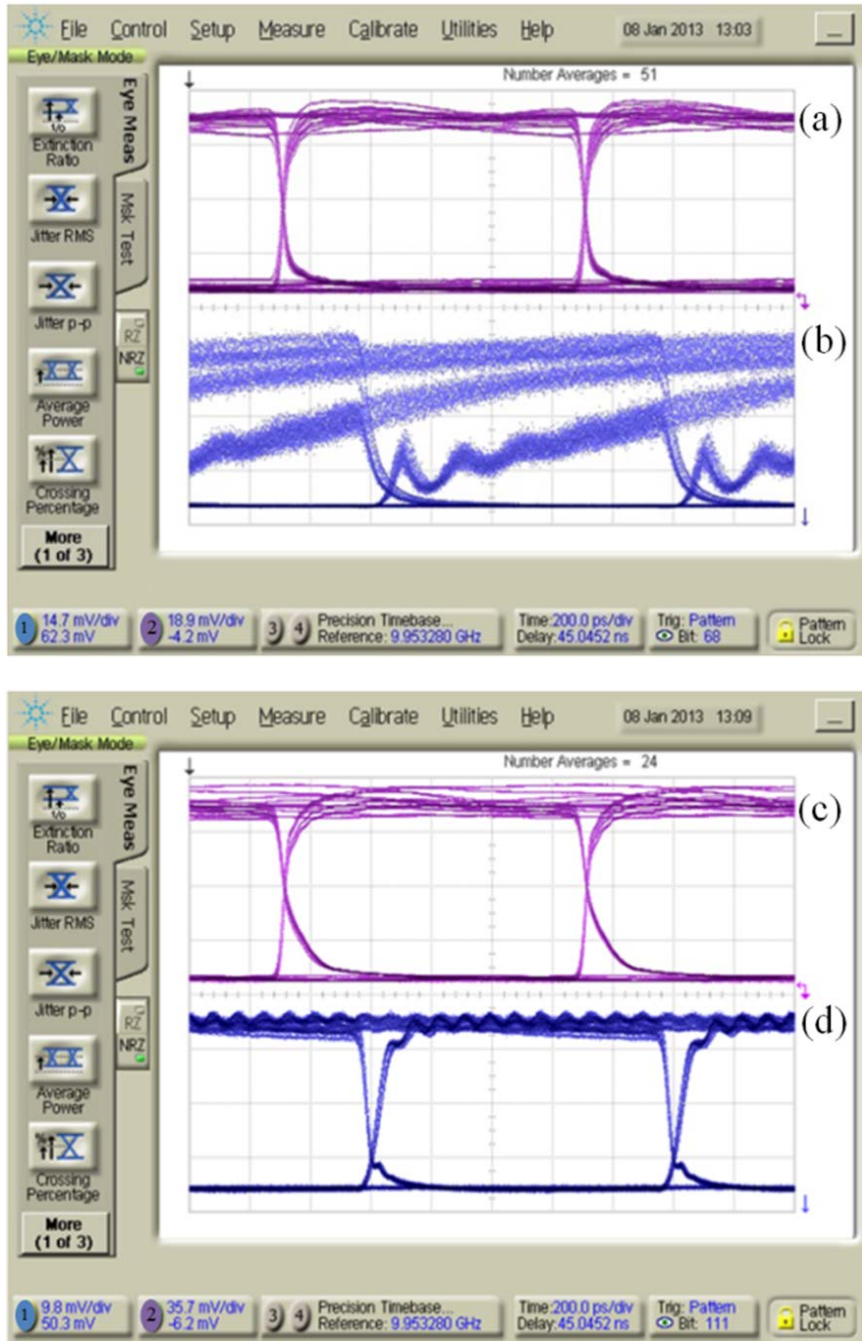


Figure 31: Left eye diagram (a) 1 Gbps PRBS input signal and (b) inverted output signal using mode suppression. Right eye diagram (c) 1 Gbps PRBS input signal and (d) inverted output signal using cavity mode shifting.

An examination of the quality of the eye diagrams verifies that the cavity-mode-shifting method of wavelength conversion provides a significant enhancement. Once

again, the mode suppression extinction ratio at 1 Gbps is distorted enough that an accurate measurement of the extinction ratio is not possible; alternatively, the 1-Gbps cavity-mode-shift eye diagram expresses a measured extinction ratio of 4.6 dB and presents an open eye indicative of a high-quality signal.

In order to test the fundamental bandwidth limitation of the cavity-mode-shift based configuration, an HP 83650A Synthesized Sweeper was used in place of the Anritsu MP1763C PPG shown in Figure 20. The sweeper was used to generate a sinusoidal signal that was provided to the external modulator. Using the same power levels and detunings utilized in the previous test, the probe beam was tested up to 19 GHz. The waveforms generated in this experiment can be seen in Figure 32.

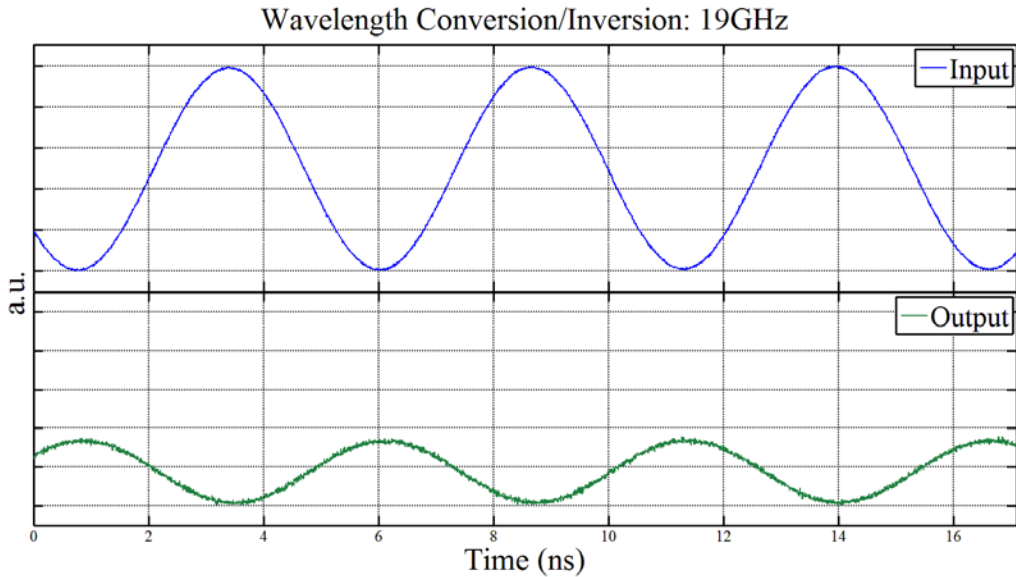


Figure 32: Probe beam wavelength conversion/inversion using a 19 GHz sinusoid.

The output of this logic gate presents a 10-dB loss in power. With the bandwidth limitation of the SMA cables usually cited at approximately 18 GHz and the 3-dB

bandwidth of the external modulator at 20 GHz, these equipment limitations may contribute to the large reduction in power. Considering these limitations, literature suggests that a decrease in cavity length can increase the data rate, as suggested in Figure 11. As suggested when examining the results of the mode-suppression method, cavity-mode shifting can also be improved by the reducing the length of the slave laser cavity [13].

4.3 NOR Gate Results

Expanding on the idea of cavity mode shifting, it is also feasible to create an optical NOR gate using a similar technique with the addition of another single-mode data laser. The laboratory setup in Figure 20 was modified to the setup shown in Figure 21. Implementing this design required that both data lasers, when injected, were capable of inducing a sufficient cavity-mode shift independently of the other data laser; additionally, simultaneous injection must cause the mode shift and a subsequent reduction in output power at the filtered mode to occur. The data beam used for the wavelength conversion experiments, referred to as “Data 1”, was changed to 1544.602 nm, corresponding to a detuning wavelength of 0.138 nm (-18.10 GHz). The injection ratio was changed to -2.08 dB (0.62 times adjacent mode). The second master beam, referred to as “Data 2”, was given an injection ratio of -10.21 dB (0.09 times) and was injected at 1547.98 nm, corresponding to a detuning of 0.148 nm (-18.03 GHz). The probe beam remained at the same detuning and injection ratio as in the previous experiments. The optical spectrum of the four different logical states is displayed in Figure 33.

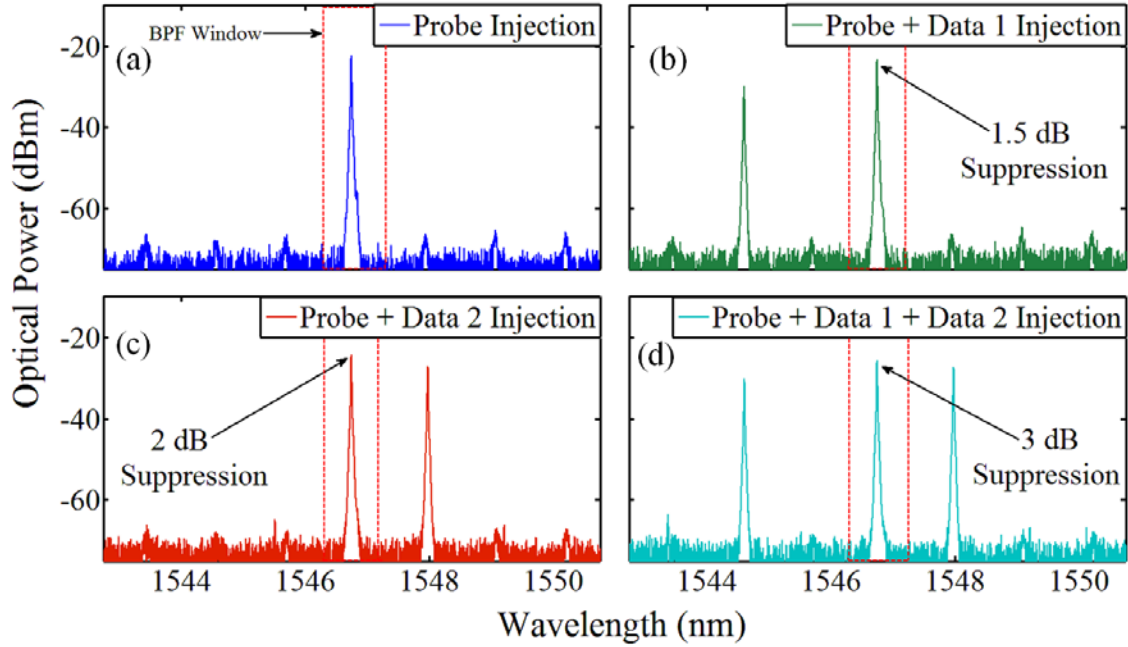


Figure 33: Optical spectrum of NOR gate. Injected lasers indicated in legend induce the following logical outputs: (a) ‘1’, (b) ‘0’, (c) ‘0’, and (d) ‘0’.

When both data beams are low the output is logic ‘1’, corresponding with the first row of the logic table presented in Figure 34. In all other instances, injection of either a single data beam or multiple data beams cause a logic ‘0’ to be transmitted.

To test this configuration in the time-domain, the pulse pattern generator was used to generate a square wave pattern with a bit rate of 12 Gbps. The experimental results can be seen in Figure 34 where an all-optical NOR gate is demonstrated at 12 Gbps.

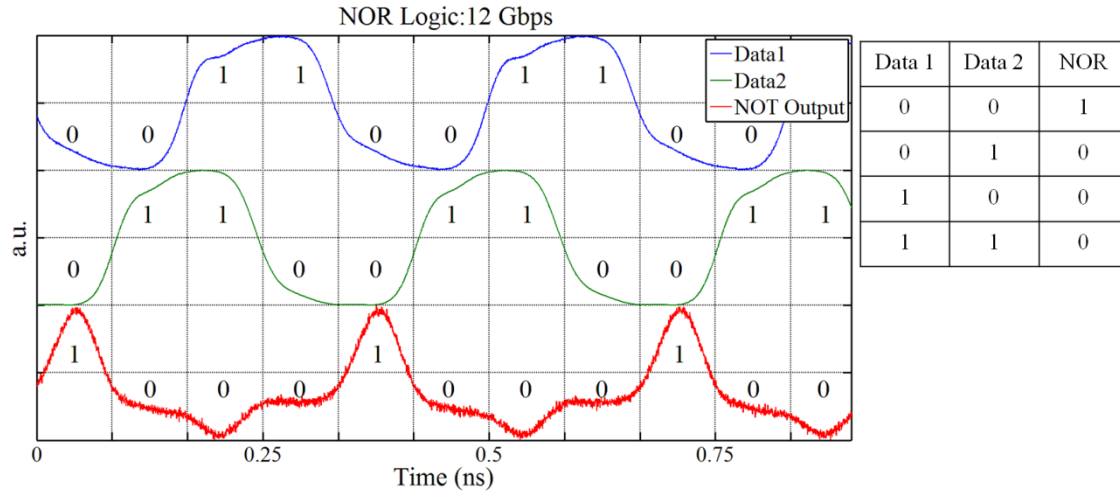


Figure 34: Input signals and output of all-optical NOR gate.

The frequency content of a 12-Gbps square wave includes harmonics at 6 and 18 GHz.

As observed in Figure 32, frequencies approaching 19 GHz experience attenuation; therefore, the output observed does not exhibit a well-defined square shape.

Additionally, the qualities of the modulated inputs also begin to diminish at 12 Gbps similar to the waveforms in Figure 29 and Figure 30. In light of the signal quality, the output demonstrated the desired NOR logic as designed by the input settings.

The NOR output waveform in Figure 34 displays an obvious logic ‘1’ state, but has three slightly different logic levels representing a logic ‘0’ output. These levels correspond to the three different laser combinations that induce a logic level of ‘0’. When the first input, referred to in Figure 33 and Figure 34 as “Data 1”, is injecting, the output produces a logic ‘0’ and does not experience the same level of suppression as in the other cases. This effect is apparent in both the optical spectrum of Figure 33 and the waveform observed in Figure 34. When both lasers are injecting, the output power level in both the optical spectrum and time domain experiences the greatest

suppression. This is an intuitive result given that the injection of two lasers will induce a greater cavity-mode shift than a single laser injection. The tiered output observed here is not detrimental considering the logic '1' level and logic '0' levels are sufficiently separated so that proper thresholding at the receiver can interpret the intended logic.

4.4 NAND Gate Results

Injection of two data carrying signals, each capable of creating a cavity-mode shift independently, is a sufficient means of generating an all-optical NOR gate. The settings of these data lasers could be altered in such a way that when injected independently there was an insignificant cavity mode shift, but a shift did occur when both lasers were injected. This resulted in a NAND operation. The equipment setup used in creating an all-optical NOR gate, illustrated by Figure 21, is used to generate a NAND gate. The only modifications made are to the detuning wavelengths and injection strengths of the data beams.

Data 1 was changed to 1545.59 nm, corresponding to a detuning wavelength of 0.158 nm (-15.52 GHz); this new wavelength actually corresponds to the mode located immediately before the central mode at which the BPF is placed. The output power of this mode is much higher than the previously mode, allowing for a greater difference in power between the injected beam and free-running mode. The injection ratio was changed to -14.82 dB (0.03 times the adjacent mode). The second master beam, referred to as Data 2, was given an injection ratio of -16.15 dB (0.02 times) and was injected at 1547.84 nm, corresponding to a detuning of 0.124 nm (-19.84 GHz).

To realize the logic, the probe beam was altered as well. The probe beam was tuned to 1546.71 nm, corresponding to a detuning of 0.009 nm (-1.25 GHz), and given an injection ratio of -14.8 dB (0.03 times) with respect to the adjacent mode. The optical spectrum of the four different logical states is displayed in Figure 35.

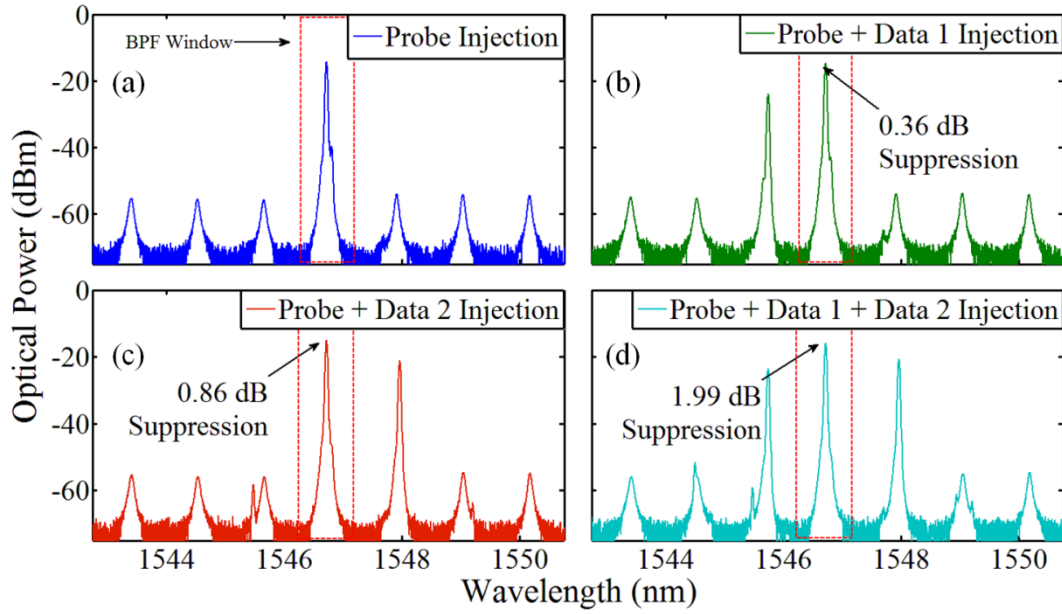


Figure 35: Optical spectrum of NAND gate. Injected lasers indicated in legend induce the following logical outputs: (a) ‘1’, (b) ‘1’, (c) ‘1’, and (d) ‘0’.

As illustrated, when both data beams are high the output is logic ‘0’, corresponding to the last row of the logic table presented in Figure 36. In all other instances, injection of either a single data beam or multiple data beams cause a logic ‘0’ to be transmitted.

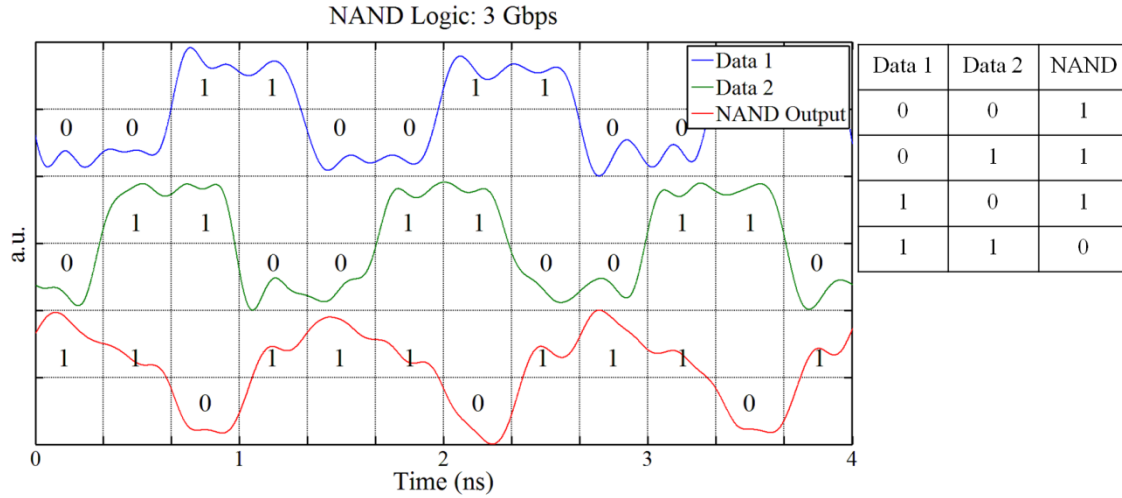


Figure 36: Input signals and output for all-optical NAND gate at 3 Gbps.

The experiments performed to investigate the NAND gate achieve a maximum data rate of 3 Gbps while at higher data rates the quality of the output diminished significantly. The injection parameters used were tuned/adjusted such that the lasers were at a low enough power that they lay just outside of the locking range of their adjacent mode. This allowed the Fabry–Perot laser to remain free-running when injected by the lasers individually; injection locking only occurred when both lasers were injected. As with the NOR logic, the waveform experiences a tiered output. When either of the data beams are injected, there is still a slight cavity-mode shift experienced resulting in a slight suppression of the filtered mode. This can be seen in both the time domain and wavelength domain of the experimental results. Once again with proper thresholding, the suppression experienced by the injection of both lasers can be separated and designated as a ‘0’ while the other states can be designated as a ‘1’.

4.5 Summary of Findings

The results described in this chapter reveal the experimental characteristics of the three experimental setups described in Chapter 3. The easiest of the wavelength conversion/logic inversion methods is the mode suppression. Experimentation revealed this method is limited to a bandwidth of approximately 500 Mbps due to spontaneous emission. This configuration can be improved by adding another single-mode laser and taking advantage of the shifting of the cavity modes that occurs under optical injection locking. While an additional single-mode laser is necessary to achieve this effect, the result is a bandwidth of approximately 19 GHz. Further exploiting the cavity-mode shifting technique, an additional data-carrying single-mode laser can be added to achieve NOR and NAND logic, which have been demonstrated at 12 Gbps and 3 Gbps, respectively. These all-optical logic gates have a bandwidth of approximately 18 GHz and 4.5 GHz, respectively.

5. Conclusions and Recommendations

This chapter highlights the research encompassed in this document by summarizing the research and results observed. This includes a description of the significance of this research and its relevance and applicability to established communication applications. Additionally, recommendations are made as to possible avenues of development pertaining to all-optical signal processing. It is the objective of this chapter to provide examples of future contributions this research may afford as well as various areas of interest that may be exploited by further investigation.

5.1 Conclusions of Research

Traditional optical wavelength conversion requires the signal be converted from an optical signal carried on some initial wavelength, to an intermediate electrical signal before it is then modulated onto a second carrier wavelength. Current methods of wavelength conversion necessitate that the initial signal be sent to a high-speed photodiode where it is converted to an electrical signal. This signal, before being sent to an external modulator, must be amplified in order to provide a significant modulation depth to the external modulator. Only then can the signal be placed on to the desired wavelength by the external modulator. The methods described here remove the need for an optical-to-electrical-to-optical conversion, eliminating expensive and often bandwidth-limited components. The wavelength conversion contribution of this research has the potential to modify the methods used by our current communication infrastructure which transfers optical data from one carrier wavelength to another. By means of optical injection locking of Fabry–Perot

semiconductor lasers and proper filtering of the desired output wavelength it is possible to achieve wavelength conversion and logic inversion. The simplest method of achieving this effect is through the use of mode suppression where by wavelength conversion can occur requiring only a Fabry–Perot laser, BPF, and an optical circulator. Implementing this method of wavelength conversion would be incredibly simple in a real-world application as it would require only the addition of a Fabry–Perot slave laser and an optical BPF. In order to convert between selected ITU bands, it would require that the Fabry–Perot selected have cavity modes that would fall on both of those ITU bands. Amplification of the injected light may be required to properly adjust input power. This solution could be implemented as an “on-chip” packaged device, making this a modular device that could be swapped and replaced based on the user’s needs. Compared to an optical-to-electrical-to-optical conversion, this implementation would be far superior for low-data-rate applications.

Wavelength conversion can be improved by adding another single-mode laser and taking advantage of the shifting of the cavity modes that occurs under optical injection locking. While an additional single-mode laser is necessary to achieve this effect, the result is a bandwidth of approximately 19 GHz. Altogether, the required equipment to perform this step include the slave Fabry–Perot laser, optical BPF, a CW probe laser, and possibly an optical amplifier. Once again, assembling these devices into a packaged “on-chip” design that is easily connected or replaced could make this an affordable and realistic solution. For low-speed applications, the mode-suppression method may be sufficient, but in order to achieve higher data rates a

second laser will be required; this solution still remains favorable when compared with the optical-electrical-optical method of wavelength conversion.

Apart from the wavelength-conversion aspects of the experiments, optical logic also presents interesting ramifications for future technologies. Utilizing the shift in the Fabry–Perot modes that occurs upon optical injection, all-optical NOR and NAND logic can be achieved. The experiments described in this document provide an initial step towards moving computations from the electronic domain to the photonic domain. The implementation of all-optical logic opens avenues towards removing electrically driven bandwidth constraints on chip-to-chip data routing/processing and logic, potentially increasing maximum achievable data rates.

In conclusion, the purpose of this manuscript is to provide useful insight and further experimental evidence of the feasibility of all-optical wavelength conversion and all-optical logic. With any luck, the addition of the work documented here will complement other research efforts concerning these disciplines and will help to provide future advancements in technology.

5.2 Contributions

- Implemented two methods of all-optical wavelength conversion and logic inversion: mode suppression dependent and cavity mode shift dependent.
- Experimentally determined an approximate upper data rate limit of mode suppression method to be 500 Mbps.

- Experimentally determined approximate upper data rate limit of cavity mode shift method to be 12.5 Gbps/ 19 GHz (laboratory equipment maximum).
- Demonstrated all-optical NOR gate based on cavity mode shifting with upper data rate limit of 12.5 Gbps (laboratory equipment maximum).
- Demonstrated all-optical NAND gate based on cavity mode shifting with upper data rate limit of 3 Gbps.

5.3 Recommendations for Future Research

There are several ways in which the research presented in this manuscript could be advanced and this section serves to present those possible areas of interest. Most of the research avenues discussed here consist of experiments that were intended to be included in this research but were abdicated due to time constraints or equipment limitations. While they are certainly not comprehensive, the examples provided here will help clarify paths forward based on the findings of this research.

Since the mode-suppression method of wavelength conversion requires fewer components compared to the cavity-mode-shifting technique, this would be the preferred method of implementing all-optical wavelength conversion in a real-world application. While the methodology described here found a data limit using these specific components and configurations, the underlying physical constraints of this method were only discussed theoretically. In order to better improve this method of wavelength conversion/data inversion, further investigations of mode suppression

should focus on determining experimentally the physical attributes that influence the speed constraints.

The NOR gate presented here worked as intended and achieved a 12.5-Gbps data rate, nearly matching the performance of the cavity-mode-shifting logic inverter as predicted. However, the NAND gate did not perform as well and only achieved a data rate of 3 Gbps. Evidence presented in the literature suggests that higher data rates are achievable [11, 47]. Time precluded further increasing the data rates of the NAND gate presented here. More time spent fine tuning the probe laser and data lasers should improve the quality of the all-optical NAND gate.

The idea of noninverting wavelength conversion is theorized and demonstrated in several articles concerning all-optical logic and switching [13, 42, 11]. Instead of the cavity mode being shifted away from the probe beam, the cavity mode can be shifted into the probe beam. This means that an input of '1' would cause the probe to lock at a different wavelength and subsequently output a '1'. As suggested in the *Literature Review* section, the idea of cavity-mode shifting can be used to impart the incoming data onto a new wavelength without inverting the bits. During experimentation this configuration was attempted, without success. Once again, time spent slowly fine-tuning the injection strength and detuning wavelengths of the probe beam and data beam should result in noninverting wavelength conversion and provide useful insight into the locking conditions. Expanding on this idea, the same change in the probe-beam conditions could achieve OR and AND logic. A NOR gate that will shift the cavity mode when either or both data signals are injecting can cause the

locking range of the cavity modes to shift towards an injected probe beam resulting in OR logic; this same method could generate an AND configuration in a similar fashion.

All of the issues previously mentioned here are outcomes that could have been achieved if the settings of both the probe beam and the data beams had been gradually altered with the effects recorded for each combination of settings. Essentially, the most comprehensive way to study each of these configurations would have been to sweep both the detuning wavelength and injection parameters of all of the lasers involved. With a complete map of the injection parameters and the subsequent outputs, it would be simple to determine the exact input parameters needed to generate an optimal output. Obviously, this would be tedious given there are up to three injected lasers each with a detuning frequency and injection ratio to adjust; a concise examination of all possible inputs would require the process be automated. Regardless of the complexity, the results would most assuredly be a constructive addition to the current field.

To broaden the experimental findings even further, the settings of the slave laser can be changed as well. As mentioned in the *Results and Analysis* section, the slave laser used in these experiments remained at a constant 20-mA bias and 20°C. This was done to simplify tuning the lasers considering there were already numerous variables involved. The bias settings and temperature of a Fabry–Perot laser certainly influence the wavelengths of the laser and the optical power of the resonant cavity modes. As with the injection parameters, the biasing and temperature parameters of the slave laser are variable, and thus could be varied to find an optimal setting for which the logic can occur.

Apart from the temperature or current settings, the actual cavity of the slave laser presents another variable that would have an effect on the wavelength switching and logic characteristics. The cavity length of the slave laser used in these experiments was 300 μm . Cavity length affects a number of laser parameters including the free-spectral range and the threshold gain. As discussed before, the speed constraint found for the mode suppression technique is not a universal limitation; by changing the laser cavity length it is possible that the long rise time associated with the regeneration of the cavity mode can be reduced. Simulations provided by Hörer and Patzak suggest the cavity-mode-shifting method can benefit from a shortened device as well [13]. As with other suggestions made in this section, an all inclusive test would require several devices to be tested which was not possible due to equipment and time limitations. Taking into consideration the quantity of variables and adjustments involved in the optical injection process, experimentally accounting for the effects of all of these attributes would provide an invaluable and comprehensive addition to the optical communication discipline.

References

- [1] R. W. Tkach and R. Essiambre, "Capacity Trends and Limits of Optical Communication Networks," *Proceedings in IEEE*, vol. 100, no. 5, pp. 1035 - 1055, May 2012.
- [2] R. Gu, Y. Qiao and Y. Ji, "Optical or Electrical Interconnects: Quantitative Comparison from Parallel Computing Performance View," in *IEEE Globecom Telecommunications Conference*, 2008.
- [3] B. Nakarmi, M. Rakib-Uddin, T. Hoai and Y. H. Won, "Demonstration of All-Optical nand Gate Using Single-Mode Fabry-Pérot Laser Diode," *Photonics Technology Letters, IEEE*, vol. 23, no. 4, pp. 236-238, February 2011.
- [4] B. E. A. Saleh and M. C. Teich, *Fundamentals of Photonics*, 2nd ed., New York: John Wiley & Sons, Inc., 2001.
- [5] E. K. Lau, L. J. Wong and M. C. Wu, "Enhanced Modulation Characteristics of Optical Injection-Locked Lasers: A Tutorial," *Selected Topics in Quantum Electronics, IEEE Journal of*, vol. 15, no. 3, pp. 618-633, May 2009.
- [6] A. Murakami, K. Kawashima and K. Atsuki, "Cavity resonance shift and bandwidth enhancement in semiconductor lasers with strong light injection," *Quantum Electronics, IEEE Journal of*, vol. 39, no. 10, pp. 1196-1204, Oct 2003.
- [7] E. K. Lau, H.-K. Sung. and M. C. Wu, "Frequency Response Enhancement of Optical Injection-Locked Lasers," *Quantum Electronics, IEEE Journal of*, vol. 44, no. 1, pp. 90-99, Jan 2008.
- [8] T. Locke, "Improvements to Optical Communication Capabilities Achieved Through the Optical Injection of Semiconductor Lasers," M.S. Thesis, Air Force Institute of Technology, Dayton, 2012.
- [9] F. Mogensen, H. Olesen and G. Jacobsen, "Locking Conditions and Stability Properties for a Semiconductor Laser with External Light Injection," *IEEE Journal of Quantum Electronics*, vol. 21, no. 7, pp. 784-793, 1985.

- [10] M. R. Uddin, J. S. Cho and Y. H. Won, "All-Optical NOR and NOT Gates at 10 Gb/s Based on Gain Modulation in Fabry-Perot Laser Diode," in *Optical Internet, 2008. COIN 2008. 7th International Conference on*, Tokyo, 2008.
- [11] H. Yoo, H. J. Lee, Y. D. Jeong and Y. H. Won, "All-optical Logic Gates using Absorption Modulation of an Injection-locked Fabry-Perot Laser Diode," in *Photonics in Switching, 2006. PS '06. International Conference on*, 2006.
- [12] M. R. Uddin, J. S. Lim, Y. D. Jeong and Y. H. Won, "All-Optical Digital Logic Gates Using Single-Mode Fabry-Pérot Laser Diode," *Photonics Technology Letters, IEEE* , vol. 21, no. 19, pp. 1468-1470, Oct 2009.
- [13] J. Hörer and E. Patzak, "Large-Signal Analysis of All-Optical Wavelength Conversion Using Two-Mode Injection-Locking in Semiconductor Lasers," *Quantum Electronics, IEEE Journal of*, vol. 33, no. 4, pp. 596-608, Apr 1997.
- [14] G. P. Agrawal, *Fiber-Optic Communication Systems*, 3rd ed., K. Chang, Ed., New York: Wiley-Interscience, 2002.
- [15] D. Qian, M. F. Huang, E. Ip, Y. K. Huang, Y. Shao, J. Hu and T. Wang, "High Capacity/Spectral Efficiency 101.7-Tb/s WDM Transmission Using PDM-128QAM-OFDM Over 165-km SSMF Within C- and L-Bands," *Journal of Lightwave Technology*, vol. 30, no. 10, pp. 1540-1548, 2012.
- [16] J. T. Verdeyen, *Laser Electronics*, 3rd ed., Holonyak, Ed., New Jersey: Prentice Hal, 1995.
- [17] E. Hecht, *Optics*, 4th ed., San Francisco: Addison Wesley, 2001.
- [18] L. A. Coldren and S. W. Corzine, *Diode Lasers and Photonic Integrated Circuits*, New York: Wiley Interscience, 1995.
- [19] V. Kovanis, A. Gavrielides, T. B. Simpson and J. M. Liu, "Instabilities and chaos in optically injected semiconductor lasers," *Applied Physics Letters*, vol. 67, no. 19, pp. 2780-2782, Nov 1995.

- [20] M. C. Pochet, T. Locke and N. G. Usechak, "Generation and Modulation of a Millimeter-Wave Subcarrier on an Optical Frequency Generated via Optical Injection," *IEEE Photonics Journal*, vol. 4, no. 5, pp. 1881-1891, 2012.
- [21] S. C. Chan, S. K. Hwang and J. M. Liu, "Period-one oscillation for photonic microwave transmission using an optically injected semiconductor laser," *Optics Express*, vol. 15, no. 22, pp. 14921-14935, 2007.
- [22] S. C. Chan, "Analysis of an Optically Injected Semiconductor Laser for Microwave Generation," *Quantum Electronics, IEEE Journal of*, vol. 46, no. 3, pp. 421-428, Mar 2010.
- [23] C. Cui and S. C. Chan, "Performance Analysis on Using Period-One Oscillation of Optically Injected Semiconductor Lasers for Radio-Over-Fiber Uplinks," *IEEE Journal of Quantum Electronics*, vol. 48, no. 4, pp. 490-499, 2012.
- [24] A. Uchida, T. Heil, Y. Liu, P. Davis and T. Aida, "High-frequency broad-band signal generation using a semiconductor laser with a chaotic optical injection," *IEEE Journal of Quantum Electronics*, vol. 39, no. 11, pp. 1462-1467, Nov 2003.
- [25] A. Uchida, Y. Liu and P. Davis, "Characteristics of chaotic masking in synchronized semiconductor lasers," *IEEE Journal of Quantum Electronics*, vol. 39, no. 8, pp. 963-970, Aug 2003.
- [26] J. M. Liu, *Photonic Devices*, New York: Cambridge University Press, 2005.
- [27] K. Iwashita and K. Nakagawa, "Suppression of Mode Partition Noise by Laser Diode Light Injection," *Microwave Theory and Techniques, IEEE Transactions on*, vol. 30, no. 10, pp. 1657-1662, Oct 1982.
- [28] S. G. Berrettini, A. Simi, A. Malacarne, A. Bogoni and L. Poti, "Ultrafast integrable and reconfigurable XNOR, AND, NOR, and NOT photonic logic gate," *IEEE Photonics Technology Letters*, vol. 18, no. 8, pp. 917-919, 2006.

- [29] J. Y. Kim, J. Kang, T. Kim and S. Han, "All-Optical Multiple Logic Gates With XOR, NOR, OR, and NAND Functions Using Parallel SOA-MZI Structures: Theory and Experiment," *Journal of Lightwave Technology*, vol. 24, no. 9, pp. 3392-3399, 2006.
- [30] C. W. Son, S. H. Kim, Y. M. Jhon, Y. T. Byun, S. Lee, D. H. Woo, S. H. Kim and T. H. Yoon, "Realization of All-Optical XOR, NOR, and NAND Gates in Single Format by Using Semiconductor Optical Amplifiers," *Japanese Journal of Applied Physics*, vol. 46, no. 1, p. 232, 2007.
- [31] J. G. Provost and R. Frey, "Logic inverter based on side mode injection locking in semiconductor lasers," *Applied Physics Letters*, vol. 56, no. 1, pp. 1-3, Jan 1990.
- [32] L. Chrostowski, B. Faraji, W. Hofmann, M. C. Amann, S. Wieczorek and W. W. Chow, "40 GHz Bandwidth and 64 GHz Resonance Frequency in Injection-Locked 1.55 μm VCSELs," *IEEE Journal of Selected Topics in Quantum Electronics*, vol. 13, no. 5, pp. 1200-1208, 2007.
- [33] E. K. Lau, "High-Speed Modulation of Optical Injection-Locked," Ph.D. Dissertation, University of California, Berkeley, 2006.
- [34] H. K. Sung, H. K. Lau and M. C. Wu, "Optical Properties and Modulation Characteristics of Ultra-Strong Injection Locked Distributed Feedback Lasers," *IEEE Journal of Selected Topics in Quantum Electronics*, vol. 13, no. 5, pp. 1215-1221, 2007.
- [35] E. K. Lau, X. Zhao, H. K. Sung, D. Parekh, C. Chang-Hasnain and M. C. Wu, "Strong optical injection-locked semiconductor lasers demonstrating > 100-GHz resonance frequencies and 80-GHz intrinsic bandwidths," *Optics Express*, vol. 16, no. 9, pp. 6609-6618, 2008.
- [36] T. B. Simpson, J. M. Liu, K. F. Huang, K. Tai, C. M. Clayton, A. Gavrielides and V. Kovanis, "Cavity enhancement of resonant frequencies in semiconductor lasers subject to optical injection," *Physical Review*, vol. 52, no. 6, pp. R4383-R4351, 1995.
- [37] X. Zhao, "Optical Injection Locking on Vertical-Cavity Surface-Emitting Lasers (VCSELs)," Ph.D. Dissertation, University of California, Berkeley, 2008.

- [38] L. Y. Chan, W. Chung, P. K. A. Wai, H. Y. Tam and M. S. Demokan, "All-optical stabilisation of state of polarisation of high speed pulse train using injection-locked laser diode," *Electronics Letters*, vol. 38, no. 19, pp. 1116-1118, Sept 2002.
- [39] L. Y. Chan, W. H. Chung, P. K. A. Wai, B. Moses, Y. H. Tam and M. S. Demokan, "Simultaneous repolarization of two 10-Gb/s polarization-scrambled wavelength channels using a mutual-injection-locked laser diode," *Photonics Technology Letters, IEEE*, vol. 14, no. 12, pp. 1740-1742, Dec 2002.
- [40] H. Liu-yan, Z. Han-yi and G. Yi-li, "All-optical NOR gate based on injection-locking effect in a semiconductor laser," *Optoelectronics Letters*, vol. 4, no. 1, pp. 33-37, Jan 2008.
- [41] H. Yoo, Y. D. Jeong, Y. H. Won, M. Kang and H. J. Lee, "All-optical wavelength conversion using absorption modulation of an injection-locked Fabry-Pérot laser diode," *Photonics Technology Letters, IEEE*, vol. 16, no. 2, pp. 536-538, Feb 2004.
- [42] T. Q. Hoai, C. S. Cho, Y. D. Jeong and Y. H. Won, "Utilize absorption modulation of an injection-locked Fabry-Pérot laser diode to demonstrate all-optical multi-wavelength conversion," in *Communications and Electronics, 2008. ICCE 2008. Second International Conference on*, Hoi An City, Vietnam, 2008.
- [43] L. Y. Chan, K. K. Qureshi, P. K. A. Wai, B. Moses, L. F. K. Lui, H. Y. Tam and M. S. Demokan, "All-optical bit-error monitoring system using cascaded inverted wavelength converter and optical NOR gate," *Photonics Technology Letters, IEEE*, vol. 15, no. 4, pp. 593-595, Apr 2003.
- [44] Y. D. Jeong, Y. H. Won and J. H. Yoon, "Tunable single-mode Fabry-Pérot laser diode using a built-in external cavity and its modulation characteristics," *Optoelectronics Letter*, vol. 31, no. 17, pp. 2586-2588, 2006.
- [45] M. R. Uddin and Y. H. Won, "All-Optical Wavelength Conversion by the Modulation of Self-Locking of a Single-Mode FP-LD," *IEEE Photonics Technology Letters*, vol. 22, no. 5, pp. 290-292, 2010.

- [46] B. Nakarmi, M. R. Uddin, T. Q. Hoai and Y. H. Won, "Demonstration of All-Optical nand Gate Using Single-Mode Fabry-Pérot Laser Diode," *Photonics Technology Letters, IEEE*, vol. 23, no. 4, pp. 236-238, Feb 2011.
- [47] B. Nakarmi, M. Rakib-Uddin and Y. H. Won, "Realization of all-optical multi-logic functions and a digital adder with input beam power management for multi-input injection locking in a single-mode Fabry-Pérot laser diode," *Optics Express*, vol. 19, pp. 14121-14129, 2011.
- [48] B. Nakarmi, M. R. Uddin, T. Q. Hoai and Y. H. Won, "All-optical logic gates (NAND and AND) based on multi-injection in single mode Fabry-Pérot Laser," in *Lasers and Electro-Optics (CLEO), 2011 Conference on*, Baltimore, 2011.
- [49] B. Nakarmi, M. R. Uddin and Y. H. Won, "All-optical exclusive-NOR and exclusive-OR logic gate based on multi-input injection locking in single mode Fabry-Pérot laser diode," *Optical Engineering*, vol. 50, no. 7, p. 075201, 2011.
- [50] B. Nakarmi and Y. H. Won, "Multi-input injection locking in a single-mode Fabry-Pérot laser for all-optical gates," *Proc. SPIE*, vol. 8284, Jan 2012.
- [51] C. M. Miller, "High-Speed Digital Transmitter Characterization Using Eye Diagram Analysis," *1266 Hewlett-Packard Journal*, vol. 45, no. 4, pp. 29-37, 1994.

REPORT DOCUMENTATION PAGE				Form Approved OMB No. 074-0188	
<p>The public reporting burden for this collection of information is estimated to average 1 hour per response, including the time for reviewing instructions, searching existing data sources, gathering and maintaining the data needed, and completing and reviewing the collection of information. Send comments regarding this burden estimate or any other aspect of the collection of information, including suggestions for reducing this burden to Department of Defense, Washington Headquarters Services, Directorate for Information Operations and Reports (0704-0188), 1215 Jefferson Davis Highway, Suite 1204, Arlington, VA 22202-4302. Respondents should be aware that notwithstanding any other provision of law, no person shall be subject to any penalty for failing to comply with a collection of information if it does not display a currently valid OMB control number.</p> <p>PLEASE DO NOT RETURN YOUR FORM TO THE ABOVE ADDRESS.</p>					
1. REPORT DATE (DD-MM-YYYY) 21-03-2013		2. REPORT TYPE Master's Thesis		3. DATES COVERED (From – To) Sept 2011 – March 2013	
4. TITLE AND SUBTITLE All-Optical Logic Gates and Wavelength Conversion Via the Injection-Locking of a Fabry–Perot Semiconductor Laser				5a. CONTRACT NUMBER	
				5b. GRANT NUMBER	
				5c. PROGRAM ELEMENT NUMBER	
6. AUTHOR(S) Harvey, Evan P., Second Lieutenant, USAF				5d. PROJECT NUMBER	
				5e. TASK NUMBER	
				5f. WORK UNIT NUMBER	
7. PERFORMING ORGANIZATION NAMES(S) AND ADDRESS(S) Air Force Institute of Technology Graduate School of Engineering and Management (AFIT/EN) 2950 Hobson Way, Building 640 WPAFB OH 45433				8. PERFORMING ORGANIZATION REPORT NUMBER AFIT-ENG-13-M-23	
9. SPONSORING/MONITORING AGENCY NAME(S) AND ADDRESS(ES) Air Force Research Laboratory Sensors Directorate (AFRL/RYPDH) Dr. Nicholas G. Usechak, Research Engineer 2241 Avionics Circle, Area B Bldg 620 WPAFB OH 45433				10. SPONSOR/MONITOR'S ACRONYM(S) AFRL/RYPDH	
				11. SPONSOR/MONITOR'S REPORT NUMBER(S)	
12. DISTRIBUTION/AVAILABILITY STATEMENT APPROVED FOR PUBLIC RELEASE; DISTRIBUTION UNLIMITED					
13. SUPPLEMENTARY NOTES This material is declared a work of the U.S. Government and is not subject to copyright protection in the United States.					
14. ABSTRACT This work investigates the implementation of all-optical wavelength conversion and logic gates based on optical injection locking (OIL). All-optical inverting, NOR, and NAND gates are experimentally demonstrated using two distributed feedback (DFB) lasers, a multi-mode Fabry–Perot laser diode (MMFP-LD), and an optical band-pass filter (BPF). The DFB lasers are externally modulated to represent logic inputs into the cavity of the MMFP-LD slave laser. The master lasers' wavelengths are aligned with the longitudinal modes of the MMFP-LD slave laser and their optical power is used to modulate the injection conditions in the slave laser. The optical BPF is used to select the longitudinal mode that is suppressed or transmitted given the logic state of the injecting master laser signals. When the input signal(s) is (are) in the on state, injection locking, and thus the suppression of the non-injected Fabry–Perot modes, is induced, yielding a dynamic system that can be used to implement photonic logic functions. Additionally, all-optical photonic processing is achieved using the cavity mode shift produced in the injected slave laser under external optical injection. The inverting logic case can also be used as a wavelength converter — a key component in advanced wavelength-division multiplexing networks. The result...					
15. SUBJECT TERMS Injection-locked lasers; Semiconductor lasers; optical logic; wavelength conversion; Fabry–Perot;					
16. SECURITY CLASSIFICATION OF:			17. LIMITATION OF ABSTRACT	18. NUMBER OF PAGES	19a. NAME OF RESPONSIBLE PERSON
a. REPORT	b. ABSTRACT	c. THIS PAGE			Pochet, Michael C., Maj., USAF
U	U	U	UU	112	19b. TELEPHONE NUMBER (Include area code) (937) 255-6565, x 4393 (michael.pochet@afit.edu)

